HHS Public Access

Author manuscript

Bioorg Med Chem. Author manuscript; available in PMC 2022 January 01.

Published in final edited form as:

Bioorg Med Chem. 2021 January 01; 29: 115887. doi:10.1016/j.bmc.2020.115887.

The 3-D Conformational Shape of *N*-Naphthyl - cyclopenta[*d*]pyrimidines Affects Their Potency as Microtubule Targeting Agents and Their Antitumor Activity

Weiguo Xiang[†], **Tasdique M. Quadery**[†], **Ernest Hamel**[£], **Lerin R. Luckett-Chastain**[€], **Michael A. Ihnat**[€], **Susan L. Mooberry**[*,§,‖], **Aleem Gangjee**[*,†,‖]

[†]Division of Medicinal Chemistry, Graduate School of Pharmaceutical Sciences, Duquesne University, 600 Forbes Avenue, Pittsburgh, PA 15282.

[£]Screening Technologies Branch, Developmental Therapeutics Program, Division of Cancer Treatment and Diagnosis, Frederick National Laboratory for Cancer Research, National Cancer Institute, National Institutes of Health, Frederick, MD 21702.

[€]Department of Pharmaceutical Sciences, The University of Oklahoma College of Pharmacy, Oklahoma City, OK 73117.

[§]Department of Pharmacology, Mays Cancer Center, University of Texas Health Science Center at San Antonio, 7703 Floyd Curl Drive, San Antonio, TX 78229.

Abstract

A series of methoxy naphthyl substituted cyclopenta[*d*]pyrimidine compounds, **4–10,** were designed and synthesized to study the influence of the 3-D conformation on microtubule depolymerizing and antiproliferative activities. NOESY studies with the *N*,2-dimethyl-*N*-(6′-methoxynaphthyl-1′-amino)-cyclopenta[*d*]pyrimidin-4-amine (**4**) showed hindered rotation of the naphthyl ring around the cyclopenta[*d*]pyrimidine scaffold. In contrast, NOESY studies with *N*,2-dimethyl-*N*-(5′-methoxynaphthyl-2′-amino)-cyclopenta[*d*]pyrimidin-4-amine (**5**) showed free rotation of the naphthyl ring around the cyclopenta[*d*]pyrimidine scaffold. The rotational flexibility and conformational dissimilarity between **4** and **5** led to a significant difference in biological activities. Compound **4** is inactive while **5** is the most potent in this series with potent microtubule depolymerizing effects and low nanomolar IC_{50} values *in vitro* against a variety of cancer cell lines. The ability of **5** to inhibit tumor growth *in vivo* was investigated in a U251 glioma xenograft model. The results show that **5** had better antitumor effects than the positive

[*]To whom correspondence should be addressed. For A.G.: phone, 412-396-6070; fax, 412-396-5593; gangjee@duq.edu. For S.L.M.: phone, 210-567-4788; fax, 210-567-4300; mooberry@uthscsa.edu.

[‖]Author Contributions

A.G. and S.L.M. contributed equally to this manuscript.

ASSOCIATED CONTENT

[*]Supporting Information

Elemental Analysis. This material is available free of charge via the Internet at http://pubs.acs.org.

The authors declare no competing financial interest.

control temozolomide and has identified **5** as a potential preclinical candidate for further studies. The influence of conformation on the microtubule depolymerizing and antitumor activity forms the basis for the development of conformation-activity relationships for the cyclopenta[*d*]pyrimidine class of microtubule targeting agents.

Graphical Abstract

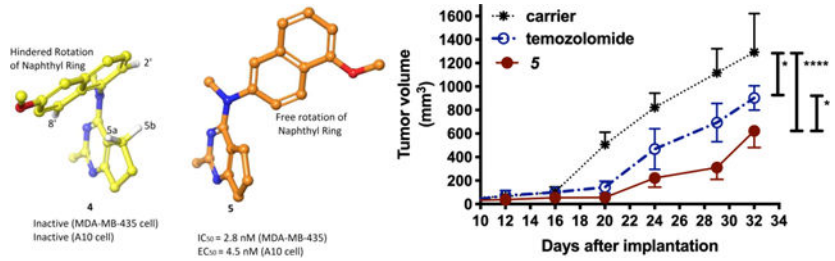

Keywords

Microtubule Depolymerizers; Microtubule Targeting Agents; Cyclopenta[*d*]pyrimidine; Antitumor Activity; Structure-Activity Relationships

1. Introduction

Microtubules are dynamic cellular structures formed by the polymerization of αβ-tubulin heterodimers in a polarized longitudinal manner to form protofilaments that associate laterally to form a tubule.[1, 2] Microtubules play essential roles in intracellular trafficking and transport, cellular migration and mitosis.[3] The ability of diverse natural products to bind directly to tubulin/microtubules and inhibit microtubule dynamics led to the development of several successful microtubule targeting anticancer drugs.[3] Microtubule targeting agents (MTAs) (Figure 1) inhibit microtubule dynamics to alter cellular microtubules and their diverse functions in both mitosis and interphase.[2, 4, 5] MTAs can be divided into two major classes, microtubule stabilizers that promote tubulin polymerization and increase the density of cellular microtubules and microtubule destabilizers that inhibit tubulin polymerization and cause loss of cellular microtubules. Clinically utilized microtubule stabilizers include the taxanes, paclitaxel, docetaxel and carbazitaxel, as well as the epothilone, ixabepilone. The clinically active microtubule stabilizers all bind within the taxane site in the lumen of microtubules.[3, 6] A second microtubule stabilizer binding site was identified, the laulimalide/peloruside A site, that is localized at the exterior surface of the microtubule.[7] Although peloruside A had promising antitumor effects in multiple xenograft models, it has not yet been evaluated clinically due to challenges in supply.[8] The first microtubule destabilizing agents identified were plant-derived, colchicine and the vinca alkaloids. These compounds defined two discrete tubulin binding sites, the colchicine and vinca sites, respectively. [6] The vinca site is located on β-tubulin at the inter-dimer interface between two tubulin heterodimers. Multiple vinca site binding drugs have found clinical utility including vincristine, vinblastine, vinorelbine and eribulin.[3] Compounds that bind to this site have additionally found utility as the payloads of antibody drug conjugates.[9] The colchicine site is a deep pocket in β-tubulin located near its interface with α-tubulin within a tubulin

heterodimer.[6] A wide variety of natural and synthetic compounds bind within this site, including colchicine and combretastatin A-4.[10, 11] Multiple colchicine site agents have been evaluated for anticancer activities in preclinical models and in clinical trials, but, to date, none have provided sufficient activity with acceptable toxicities to obtain FDA approval for anticancer indications. The major challenge in the field has been to develop an FDA-approved colchicine site agent for anticancer indications. Two additional microtubule destabilizer sites on tubulin were recently identified, the maytansine and pironetin sites.[6] A maytansine analog has found utility as the payload of an antibody drug conjugate Kadcyla®, which is approved to treat advanced HER2-positive breast cancer.[12]

The success of clinically used MTAs, including taxanes and vincas, are hampered by innate and acquired drug resistance.[3, 13] Two well-established drug resistance mechanisms include the expression of the ABC transporter, P-glycoprotein (Pgp) that functions as a drug efflux pump and the expression of the βIII-isotype of tubulin that has also been associated with drug resistance to MTAs.[3, 14, 15] An advantage of many colchicine site agents is their ability to circumvent both of these clinically relevant forms of drug resistance.[16, 17] However, to date no colchicine site agent has received FDA approval for anticancer indications,[6] attesting to the necessity to develop viable colchicine site agents for evaluation as potential cancer chemotherapeutic drugs.

2. Rationale

We[18] reported compound **1** (Figure 2A) as a potent antiproliferative (IC_{50} = 25.7 nM) and microtubule depolymerizing agent (EC_{50} = 282 nM), while its corresponding N4-desmethyl analog **2** (Figure 2A) was almost inactive. The shielding effect of the phenyl on the 6-CH_3 moiety in **1** compared with **2** (δ 0.86 ppm in **1**, and 1.12 ppm in **2**) indicates that the phenyl ring in **1** resides above the cyclopenta ring and the phenyl ring in **2** resides away from the cyclopenta ring (Figure 2B). However, the dramatic difference in antiproliferative and microtubule depolymerizing activities of **1** and **2** could also be attributed to lipophilic and/or the 3-D conformational differences of the phenyl ring dictated by the N4-methyl moiety. In an attempt to influence both lipophilicity and conformational preferences, we reasoned that the addition of a napththyl ring on the N4-position along with the N4-methyl would provide increased lipophilicity as well as conformational variations. Hence, we designed a series of *N*-methyl-*N*-methoxynaphthyl cyclopenta[*d*]pyrimidin-4-amines **(4–10)** (Figure 3) based on the potent MTA **3** (IC_{50} = 7.0 nM).[19] These compounds (**4–10**) possess an N4-methyl and also have a naphthyl ring at the N4-position with different positions of attachment and location of the substitution on the naphthyl ring.

In addition, we[20, 21] have reported that the 2-position substituent influences the antiproliferative activity of similar cyclopenta[*d*]pyrimidines with microtubule depolymerizing abilities. Thus, it was of interest to also synthesize and evaluate the 2-H and 2-NH_2 substituents of selected compounds **8**–**10** to ascertain the effect of the 2-position substituent on biological activity.

Starting with the 2,4-dimethyl-4-(4′-methoxy)phenyl cyclopenta[*d*]pyrimidine **3** as the 4′-phenyl substituted analog, proposed compounds **4–10** were docked in the X-ray crystal

structure of colchicine in tubulin at the colchicine site (PDB: 4O2B,[22] 2.30 Å) using Maestro in Schrödinger.[23] All the proposed analogs **4–10** are N4-naphthyl substituted analogs. Multiple low energy conformations were obtained on docking. Figure 4 shows the docked conformation of **5** (tan) as a representative example in the colchicine site of tubulin. The cyclopenta[*d*]pyrimidine scaffold of **5** overlaps the A-ring of colchicine (cyan) and forms hydrophobic interactions at the αβ tubulin interface with Leuβ252, Leuβ255, Alaβ316, Alaβ354, Ileβ318 and Ileβ378. The N1 of the cyclopenta[*d*]pyrimidine scaffold of **5** forms a hydrogen bond with a water molecule in the crystal structure that is bonded to Valβ238 and Cysβ241. The N4-CH_3 interacts with Leuβ255 through hydrophobic interactions. The 5-methoxynaphthyl ring of **5** occupies the region where the C-ring of colchicine binds, and this allows hydrophobic interactions with Alaα180, Valα181 Thrβ314 and Lysβ352 to a greater extent than **1**, which contains a N4-phenyl.

The best docked pose of compound **5** had a docked score of −7.59 kcal/mol, comparable to that of the lead compound **3** (−7.35 kcal/mol). The key binding interactions indicated by the docking study of compound **5** in the colchicine site of tubulin (Figure 4) are retained by target compounds **4** and **6**–**10** with docked scores (−8.13, −7.92, −7.43, −7.71, −6.94 and −7.25 kcal/mol, respectively) similar to that of target compound **5** (Figures S2–S6). Thus, on the basis of our molecular modeling, we anticipated potent activity of the proposed compounds as MTAs acting at the colchicine site. In addition, in keeping with previous colchicine site agents,[16] these analogs were expected to circumvent tumor resistance via both Pgp and βIII-tubulin-isotype and hence afford advantages over some currently used clinical agents like paclitaxel.[24]

3. RESULT AND DISCUSSION

3.1 Chemistry

Formyl protection of the amine in hydroxyaminonaphthalenes **11a-d** (Scheme 1) with formic acid and acetic anhydride afforded *N*-formyl hydroxynaphthylamines **12a-d**. Dimethylation of **12a-d** using sodium hydride and methyl iodide in DMF at 0 °C gave *N*-methyl-*N*-formyl methoxynaphthylamines **13a-d** in 71–90% yield in two steps. Deformylation of **13a-d** in concentrated HCl at reflux afforded *N*-methyl methoxylnaphthylamines **14a-d** in 90–95% yield. Nucleophilic displacement of 4-chlorocyclopenta[*d*]pyrimidines **15a**–**15c** (Scheme 2) by the secondary amine in compounds **14a-d** afforded target compounds **4–10** in 71–93% yield. The corresponding HCl salts of the target compounds were precipitated in MtBE in 90–97% yield.

3.2 Biological Evaluation

Compounds **3–10** were tested for their antiproliferative and cytotoxic effects against the drug sensitive MDA-MB-435 cancer cell line using a sulforhodamine B (SRB) assay as previously described[18] with CA-4 as the positive control. The microtubule depolymerizing effects of these compounds were evaluated in a cell-based phenotypic screen using A-10 cells. The data (Table 1) indicate that compound **4** had no microtubule depolymerizing activity at 10000 nM. Compound **5** was about 3-fold more potent than CA-4 in its microtubule depolymerizing activity and equipotent to CA-4 for its antiproliferative effects.

Compound **6** was more than 100-fold less potent than **5** for microtubule depolymerizing and antiproliferative activities. These results suggest that free rotation of the naphthyl ring is required for potent microtubule depolymerizing and antiproliferative effects of this class of compounds. Compound **7** was less potent than **5** and **6**, which is consistent with our previous[19] SAR that a methoxy group at the *para*-position of the aromatic ring is essential for optimal activity. The corresponding 2-H and 2-NH_2 compounds **9** and **10**, respectively, were less potent than the 2-CH_3 compound **5**, which emphasizes the importance of the 2-CH_3 group for antitubulin activity, as reported previously for compound **3** and its analogs.[18] Compound **8,** which is a 2-H analog of **4** also had no microtubule depolymerizing activity at 10000 nM.

We further tested these compounds in the U251 cancer cell line for their cytotoxic effects (Table 2). Compound **5**, the most potent analog, was 5-fold more potent than **4** and 2-fold more potent than **6** and **7** in the U251 cytotoxicity assay. Compounds **8** and **9** were 7- and 4-fold less active, respectively, than **5**.

The effects of **4–6**, **8** and **9** on the inhibition of the polymerization of purified tubulin were evaluated (Table 3). This allows for a study of the direct interaction of these compounds with their intracellular target. The ability of these compounds to bind to the colchicine site on tubulin was evaluated by measuring inhibition of [^{3}H]colchicine binding to tubulin. The data show that **3**, **5–6** and **9** were effective and potent inhibitors of tubulin assembly and that at 1 μM and 5 μM concentrations, **3**, **5** and **9** strongly inhibited the binding of [^{3}H]colchicine, comparable to the inhibition observed with the standard CA-4. It is therefore likely that **3**, **5** and **9** bind to the colchicine site on tubulin. However, since the colchicine binding studies were not performed at equilibrium, we are unable to make specific conclusions about relative affinities of these compounds for tubulin. In contrast to **5**, compounds **4** and **8** had IC_{50} values > 20 μM in the tubulin assembly assay. Compound **6** had reduced inhibitory activity as compared with **3**, **5** and **9**. The corresponding 2-H compound **9** had less colchicine inhibitory activity as compared with the 2-CH_3 compound **5**.

3.3 Conformational Study and Molecular Modeling

Compounds **4**–**10** possess comparable docking scores in silico[23] in the colchicine site of tubulin. However, the inactivity of compounds **4** and **8** in the microtubule depolymerization assay and the colchicine binding assay prompted us to conduct a conformational study to decipher possible reasons for the *in vitro* inactivity of **4**.

In **4** and **6**, the two 5-position protons have different chemical shifts (Figure 5) in the ^{1}H NMR, indicating a restricted rotation of the naphthyl ring as the two 5-position protons are under different influences of the naphthyl ring. However, in **5**, the chemical shifts of the two 5-position protons are identical. This suggests free rotation of the 5-methoxynaphthyl ring in **5**,[19] in that both 5-position protons are equally influenced by the anisotropy of the naphthyl ring in **5**.

We conducted a conformational search of compounds **4** and **5** using MacroModel in Schrödinger.[23] The number of conformations within 5 kcal/mol obtained for **4** and **5** were 15

and 29 respectively. This suggests compound **4** to be a conformationally restricted analog compared with **5**.

In order to better understand the spatial relationship of the 5-position protons with the naphthyl ring protons, we conducted NOESY experiment for compounds **4**, **5** and **6**.[25–28]

In the NOESY spectrums of **4** (Figure 6A), only one of the 5-position protons (5a) resides in the NOE effective range of the 8′-proton, but not the 2′-proton. The other 5-position proton (5b) resides in the NOE effective range of the 2′-proton, but not the 8′-proton. If the naphthyl ring could rotate freely around the cyclopenta[*d*]pyrimidine via the N4-C1′ bond and the C4-N4 bond, the two 5-position protons would reside in an identical chemical environment (chemical shift) and have an identical spatial relationship with both the 2′- and 8′-protons. Hence, in **4** the NOESY experiment suggests a hindered rotation of the naphthyl ring around the cyclopenta[*d*]pyrimidine scaffold, under conditions in which the study was conducted (room temperature, DMSO and D_2O solution).

In compound **5** (Figure 6B), both 5-position protons lie within the range of NOE effect of both 1′ and 3′ protons on the naphthyl ring. These data, together with overlapped peaks of the 5-position protons in ^1H NMR, suggest that the naphthyl ring resides above the 5-position protons and that the σ-bonds (C4-N4 and N4-C2') are freely rotatable in **5**.

In compound **6** (Figure 6C), both 5-position protons reside in the NOE effective range of the 2′- and 8′-protons. However, unlike in **5**, the two 5-position protons in **6** are not identical. This suggests partially or slowly rotatable σ-bonds (C4-N4 and N4-C1′) in **6**.

The intensity of NOE cross peaks is a direct indication of inter-proton spatial distance. Based upon a reference NOE peak corresponding to a known distance, the distance of other protons can be calculated. The following equation measures the relationship of NOE intensities and inter-proton distances: $R = Rref\sqrt[6]{\frac{Iref}{I}}$.[29] In this equation, R is the distance of protons; I is the intensity of the NOE peak; $Rref$ and $Iref$ are the distance and intensity of the reference protons, respectively.

We integrated the NOESY spectra of **4–6** (Figure 7) and calculated the spatial distances between the 5-position protons and the protons on the naphthyl ring, using two protons on the naphthyl ring as a reference peak. The lowest energy conformations of **4–6** were also calculated by Maestro in Schrödinger.[23] The result demonstrated that the minimum energy conformation of compound **4** in DMSO/D_2O solution extrapolated from NOESY is close to the conformation predicted by Maestro in silico (Figure 7). For compounds **5** and **6**, a discrepancy between the NOE conformation and the Maestro predicted minimum energy conformation was observed. This is probably due to the fact that **5** and **6** exist in multiple stable conformations and NOESY only shows the cumulative effects of these multiple conformations.

Figure 8 shows the docked pose of compound **4** in the colchicine site of tubulin. The lowest energy conformations of compounds **4** and **5** are different from the corresponding predicted docked conformations of the compounds in the colchicine site of tubulin.

We superimposed the lowest energy conformations and the docked conformations of compounds **4** and **5** by overlapping the cyclopenta[*d*]pyrimidine rings of the compounds (Figure 9). The image illustrates that, for both **4** and **5**, the naphthyl ring needs to rotate around the cyclopenta[*d*]pyrimidine ring, from its lowest energy conformation to attain the docked conformation.

We calculated the rotational energy barrier from the minimum energy conformation to the docked conformation of compounds **4** and **5** using MacroModel in Schrödinger.[23] For compound **4**, the rotational energy barrier was found to be > 8.4 kcal/mol, whereas, for compound **5**, the rotational energy barrier was found to be < 8.4 kcal/mol. Thus, we propose that the higher rotational energy barrier for compound **4** favors the energy minimized conformation and is unable to attain the docked conformation. Compound **5**, however, can freely rotate from its energy minimized form to obtain its docked conformation in the colchicine site of tubulin.

It is this rotational energy barrier that could explain the fact that compound **4** was inactive whereas compound **5** was found to be the most potent compound in this series. Figures S2A and S2B illustrate the rotational energy barrier for compounds **4** and **5**, respectively.

Thus, the lower activity of **4** can be attributed, in part, to the higher energy barrier to adopt the bound conformation in the colchicine binding site compared with the most potent analog **5** with a lower energy barrier between the minimum energy conformation and the bound conformation.

Our purpose was to determine a minimum energy conformation, in solution, for **4** and **5** and to relate this to the energy required to bind to the colchicine site. This energy difference allows for an estimation of the energy difference between the minimum energy conformation and the bound conformation and suggests a reason for the difference in biological activity of **4** and **5** as detailed above.

One of the mechanisms of drug resistance that leads to chemotherapy failure with microtubule targeting agents is the overexpression of the βIII-isotype of tubulin.[14, 15] An isogenic HeLa cell line pair[30] was used to evaluate the effects of βIII-tubulin expression on the antiproliferative and cytotoxic activities of **5**–**7**, **9**, and **10** as compared with paclitaxel and CA-4. Compounds **5**–**7**, **9**, and **10** all displayed a relative resistance (Rr) value of 0.7 to 0.8 and CA-4 had an Rr value of 1.2 (Table 4) in this cell line pair, suggesting that they overcome drug resistance mediated by βIII-tubulin. In contrast, paclitaxel, which had an Rr of 4.7, is susceptible to resistance mediated by βIII-tubulin (Table 4). Thus, compounds **5–7**, **9** and **10** can circumvent a clinically relevant mechanism of drug resistance with advantages over paclitaxel.

In addition, the ability to circumvent Pgp-mediated drug resistance was also evaluated using an SK-OV-3 isogenic cell line pair[30] (Table 5). Cells expressing Pgp were over 800-times more resistant to paclitaxel, a known Pgp substrate, as compared with the parental cells. As with **3** and CA-4, cells with Pgp were only 1.0 to 2.1-times more resistant to compounds **5–**

7, **9** and **10**. These data indicate that **5–7**, **9** and **10** are poor substrates for Pgp and therefore may also have advantages over clinically used MTAs such as paclitaxel.

Compound **5**, the most potent microtubule depolymerization agent in the current study, was selected by the National Cancer Institute for evaluation in the NCI 60 cell line panel. It showed potent GI_{50}s against most of the NCI 60 cancer cell lines (Table S2). Moreover, compound **5** was more potent than paclitaxel (Table S3) across the NCI 60 cell line panel.

In light of its low nanomolar potency *in vitro* in the NCI 60 cell line panel and its potent microtubule depolymerization activity, compound **5** was selected for an *in vivo* xenograft study. Compound **5** was tested for *in vivo* antitumor effects in the U251 xenograft model. The effect of systemic treatment of **5** in human U251 glioma cells implanted into nude mice in comparison to the standard agent temozolomide was examined (Fig. 10). Compound **5** inhibited tumor growth as compared with the carrier or temozolomide without significant toxicity and with less toxicity than temozolomide as measured by animal weight.

4. Summary

Thus, on the basis of our results, cyclopenta[*d*]pyrimidine analog **5** not only circumvents two mechanisms of clinical drug resistance and demonstrates across the board antiproliferative activity in a wide range of cancer cells *in vitro* but also demonstrates *in vivo* antitumor activity in a U251 glioma xenograft model superior to temozolomide. In addition, the significant difference of antitubulin activity between **4** and **5** was shown, in part, to be due to conformational rigidity vs flexibility. Compound **5** is being further evaluated in preclinical studies as a potential candidate for clinical trials as an anticancer agent.

5. Experimental Section

Analytical samples were dried in vacuum (0.2 mm Hg) in a CHEM-DRY drying apparatus over P_2O_5 at 50 °C. Melting points were determined on a digital MEL-TEMP II melting point apparatus with a FLUKE 51K/J electronic thermometer and are uncorrected. Nuclear magnetic resonance spectra for protons (^{1}H NMR) were recorded on a Bruker Avance II 400 (400 MHz) or on a 500 (500 MHz) NMR system. The chemical shift values are expressed in ppm (parts per million) relative to tetramethylsilane as an internal standard: s, singlet; d, doublet; t, triplet; q, quartet; quint, quintet; m, multiplet; br, broad singlet. The coupling constants and NOE peak intensities were measured by the software MestreC and MestReNova. Thin-layer chromatography (TLC) was performed on Whatman Sil G/UV254 silica gel plates with a fluorescent indicator, and the spots were visualized under 254 and 365 nm illumination. Proportions of solvents used for TLC are by volume. Column chromatography was performed on a 230–400 mesh silica gel (Fisher Scientific) column. Elemental analyses were performed by Atlantic Microlab, Inc., Norcross, GA. Elemental compositions are within ± 0.4% of the calculated values and indicate > 95% purity of the compounds. Fractional moles of water or organic solvents found in some analytical samples could not be prevented despite 24 – 48 h of drying in vacuo and were confirmed where possible by their presence in the ^{1}H NMR spectra. HPLC-MS was analyzed with an Acquity system. A linear gradient of 90% of 0.1% formic acid in water, 10% of 0.1% formic acid in

ACN over 10 min, and then 100% ACN for 5 min was used. All final compounds were > 95% pure as established by elemental analysis, HPLC, or both. All solvents and commercial chemicals were purchased from Sigma-Aldrich or Fisher Scientific and were used as received.

General synthesis for formylation of hydroxy naphthylamine 12a-d.

Formic acid (2 eq.) and acetic anhydride (2 eq.) were stirred in dichloromethane at 0 °C for 0.5 h. The appropriate hydroxy naphthylamine (**11a-d**, 1 eq.) was added to the above solution and stirred at rt overnight.[31] The reaction mixture was diluted with EtOAc (30 mL) and washed with aqueous $NaHCO_3$ (2 × 10 mL) and water (10 mL). The organic layer was dried with 4 Å MS and concentrated with a rotatory evaporator to yield a yellow solid, which was directly used for the next step.

General synthesis for dimethylation of N-formyl hydroxylnaphthylamines 13a-d.

N-Formyl hydroxynaphthylamine **12a-d** was dissolved in DMF at −5 °C. To the above solutions, NaH (60% in mineral oil, 3 eq.) was added in portions. After 15 min., MeI (3 eq.) was added, and the reaction mixtures were stirred at the same temperature for another 4 h. The reaction was carefully quenched with water (30 mL), and EtOAc (60 mL) was added. The organic layer was separated, washed with water (3 × 20 mL), dried over Na_2SO_4 and concentrated with 1 g silica gel to directly make a dry plug. This plug was placed on the top of a silica gel column and eluted with hexanes and EtOAc. Fractions containing the product were pooled and evaporated to afford the *N*-methyl-*N*-formyl methoxynaphthylamine compounds **13a-d**.

N-Methyl-*N*-formyl 6-methoxynaphthyl-1-amine (13a).

Compound **13a** was synthesized from **11a** following the general procedure in 71% yield as a semisolid: TLC *Rf* 0.38 (Hexanes/EtOAc, 3:1); ^{1}H NMR ($CDCl_3$) δ 3.47 (s, 3H, NCH_3), 4.03 (s, 3H, OCH_3), 6.84 (d, J = 8.0 Hz, 1H, ArH), 7.28 (dd, J = 2.0 Hz, 8.0 Hz, 1H, ArH), 7.40 (m, 2H, ArH), 7.54 (d, J = 2.0 Hz, 1H, ArH), 8.31 (d, J = 8.0 Hz, 1H, ArH), 8.63 (bs, 1H, CHO); Anal. calcd. for ($C_{13}H_{13}NO_2$) C, H, N.

N-Methyl-*N*-formyl 5-methoxynaphthyl-2-amine (13b).

Compound **13b** was synthesized from **11b** following the general procedure in 79% yield as a semisolid: TLC *Rf* 0.42 (Hexanes/EtOAc, 3:1); ^{1}H NMR ($CDCl_3$) δ 3.39 (s, 3H, NCH_3), 4.03 (s, 3H, OCH_3), 6.89 (d, J = 7.2 Hz, 1H, ArH), 7.23 (d, J = 9.0 Hz, 1H, ArH), 7.59 (m, 2H, ArH), 7.61 (d, J = 2.8 Hz, 1H, ArH), 8.19 (d, J = 8.0 Hz, 1H, ArH), 8.73 (bs, 1H, CHO); Anal. calcd. for ($C_{13}H_{13}NO_2$) C, H, N.

N-Methyl-*N*-formyl 4-methoxynaphthyl-1-amine (13c).

Compound **13c** was synthesized from **11c** following the general procedure in 80% yield as a semisolid: TLC *Rf* 0.39 (Hexanes/EtOAc, 3:1); ^{1}H NMR ($CDCl_3$) δ 3.43 (s, 3H, NCH_3), 4.08 (s, 3H, OCH_3), 6.80 (d, J = 8.0 Hz, 1H, ArH), 7.57–7.92 (m, 3H, ArH), 7.74 (d, J = 7.5 Hz, 1H, ArH), 8.27 (bs, 1H, CHO), 8.36 (d, J = 9.0 Hz, 1H, ArH); Anal. calcd. for ($C_{13}H_{13}NO_2$) C, H, N.

N-Methyl-*N*-formyl 5-methoxynaphthyl-1-amine (13d).

Compound **13d** was synthesized from **11d** following the general procedure in 90% yield as a semisolid: TLC *Rf* 0.43 (Hexanes/EtOAc, 3:1); ^{1}H NMR ($CDCl_3$) δ 3.39 (s, 3H, NCH_3), 4.05 (s, 3H, OCH_3), 6.91 (d, J = 7.5 Hz, 1H, ArH), 7.39 (t, J = 8.5 Hz, 2H, ArH), 7.49–7.53 (m, 2H, ArH), 8.30 (bs, 1H, CHO), 8.34 (d, J = 8.5 Hz, 1H, ArH); Anal. calcd. for ($C_{13}H_{13}NO_2$) C, H, N.

General synthesis of methoxy N-methylnaphthylamines.

The appropriate *N*-methyl-*N*-formylmethoxynaphthylamine **13a-d** was dissolved in 10 mL concentrated HCl and kept at reflux for 2 h. The reaction mixture was cooled in an ice-water bath, and the pH was adjusted to above 12 with NH_4OH. The solution was treated with EtOAc (25 mL) and the phases separated. The organic layer was washed with water (3 × 10 mL), dried with anhydrous Na_2SO_4 and concentrated with 1 g silica gel to make a plug. This plug was placed on the top of a silica gel column and eluted with hexanes and EtOAc. Fractions containing the product were pooled and evaporated to provide the methoxy *N*-methylnaphthylamine compounds **14a-d**.

N-Methyl 6-methoxynaphthyl-1-amine (14a).

Compound **14a** was synthesized from **13a** following the general procedure in 90% yield as a pale white solid: mp 65.0–67.3 °C; TLC *Rf* 0.52 (Hexanes/EtOAc, 3:1); ^{1}H NMR ($CDCl_3$) δ 1.63 (bs, 1H, NH), 3.28 (s, 3H, NCH_3), 3.95 (s, 3H, OCH_3), 7.22 (m, 1H, ArH), 7.39 (m, 1H, ArH), 7.47 (m, 1H, ArH), 7.73 (m, 1H, ArH), 7.81 (m, 1H, ArH), 8.37(m, 1H, ArH); Anal. calcd. for ($C_{12}H_{13}NO \cdot 0.1H_2O$) C, H, N.

N-Methyl 5-methoxynaphthyl-2-amine (14b).

Compound **14b** was synthesized from **13b** following the general procedure in 93% yield as a pale white solid: mp 63.2–64.0 °C; TLC *Rf* 0.53 (Hexanes/EtOAc, 3:1); ^{1}H NMR ($CDCl_3$) δ 3.04 (s, 3H, NCH_3), 4.03 (s, 1H, NH), 4.04 (s, 3H, OCH_3), 6.62 (d, J = 7.2 Hz, 1H, ArH), 6.90 (d, J = 2.2 Hz, 1H, ArH), 6.93 (dd, J = 9.0 Hz, 2.2 Hz, 1H, ArH), 7.20 (m, 1H, ArH), 7.32 (d, J = 8.2 Hz, 1H, ArH), 8.07 (d, J = 9.0 Hz, 8.2 Hz, 1H, ArH); Anal. calcd. for ($C_{12}H_{13}NO \cdot 0.05$EtOAc) C, H, N.

N-Methyl 4-methoxynaphthyl-1-amine (14c).

Compound **14c** was synthesized from **7c** following the general procedure in 95% yield as a pale white solid: mp > 270 °C; TLC *Rf* 0.53 (Hexanes/EtOAc, 3:1); ^{1}H NMR ($CDCl_3$) δ 3.12 (s, 3H, NCH_3), 3.47 (bs, 1H, NH), 4.03 (s, 3H, OCH_3), 6.75 (m, 1H, ArH), 7.33–7.74 (m, 3H, ArH), 8.13 (d, J = 8.2 Hz, 1H, ArH), 8.31 (d, J = 8.2 Hz, 1H, ArH); HPLC > 95%; ESIMS *m/z* $[M+H]^+$, calcd 188.10, found 188.22.

N-Methyl 5-methoxynaphthyl-1-amine (14d).

Compound **14d** was synthesized from **13d** following the general procedure in 90% yield as a pale white solid: TLC *Rf* 0.52 (Hexanes/EtOAc, 3:1); ^{1}H NMR ($CDCl_3$) δ 3.04 (s, 3H, NCH_3), 4.03 (s, 3H, OCH_3), 4.42 (bs, 1H, NH), 6.68 (m, 1H, ArH), 6.86 (m, 1H, ArH), 7.39–7.43 (m, 3H, ArH), 7.72 (m, 1H, ArH); Anal. calcd. for ($C_{12}H_{13}NO$) C, H, N.

General Procedure for Nucleophilic Displacement from 4-Chlorocyclopenta[*d*]pyrimidines.—4-Chlorocyclopenta[*d*]pyrimidines **15a-c** and the appropriate methoxy *N*-methylnaphthylamine **14a-d** were dissolved in dioxane (3 mL). To this solution was added a 2 N HCl ether solution (1–2 drops). The mixture was heated at reflux for 3–6 h. Then the reaction mixture was cooled and evaporated at reduced pressure. The residue was diluted with chloroform, neutralized with NH_4OH, washed with water (2 × 10 mL), dried with anhydrous Na_2SO_4, and evaporated with 1 g silica gel under reduced pressure to give a dry plug. This plug was placed on the top of a silica gel column and eluted with $CHCl_3$ and MeOH. Fractions containing the product were pooled and evaporated to afford pure compound.

General Method for the HCl Salt from Base.—HCl ether solution (2 N) was added dropwise to a solution of the free base of **4–6** in MtBE until no further solid precipitated. The solid was collected by filtration and dried to yield the HCl salt.

N-(6'-methoxynaphthyl-1')-N,2-dimethyl-cyclopenta[d]pyrimidin-4-amine hydrochloric acid salt (4·HCl).: 86% yield, off-white solid. mp 233.4–233.9 °C; TLC *Rf* 0.63 ($CHCl_3$/MeOH/TEA, 10:1:0.1); ^{1}H NMR (DMSO-d_6) δ 1.02 (m, 1H, CH_2), 1.56 (m, 3H, CH_2), 2.57 (s, 3H, 2-CH_3), 2.87 (m, 2H, CH_2), 3.65 (s, 3H, NCH_3), 3.91 (s, 3H, OCH_3), 7.26 (dd, J = 2.4 Hz, 6.79 Hz, 1H, ArH), 7.46 (d, J = 7.0 Hz, 1H, ArH), 7.53 (d, J = 2.4 Hz, 1H, ArH), 7.57 (t, J = 8.0 Hz, 1H, ArH), 7.64 (d, J = 9.0 Hz, 1H, ArH), 7.99 (d, J = 8.0 Hz, 1H, ArH), 14.90 (bs, 1H, NH^+); Anal. calcd. for ($C_{20}H_{22}ClN_3O\cdot 0.25H_2O$) C, H, N, Cl.

N-(5'-methoxynaphthyl-2')-N,2-dimethyl-cyclopenta[d]pyrimidin-4-amine hydrochloric acid salt (5·HCl).: 91% yield, off-white solid. mp 222.3–222.5 °C; TLC *Rf* 0.62 ($CHCl_3$/MeOH/TEA, 10:1:0.1); ^{1}H NMR (DMSO-d_6) δ 1.69–1.71 (m, 4H, CH_2), 2.56 (s, 3H, 2-CH_3), 2.85 (m, 2H, CH_2), 3.66 (s, 3H, NCH_3), 4.00 (s, 3H, OCH_3), 7.07 (d, J = 7.2 Hz, 1H, ArH), 7.57 (m, 3H, ArH), 7.93 (d, J = 2.0 Hz, 1H, ArH), 8.23 (d, J = 9.0 Hz, 1H, ArH); Anal. calcd. for ($C_{20}H_{22}ClN_3O\cdot 0.25H_2O$) C, H, N, Cl.

N-(4'-methoxynaphthyl-1')-N,2-dimethyl-cyclopenta[d]pyrimidin-4-amine (6).: 76% yield, off-white solid. mp 145.1–145.6 °C; TLC *Rf* 0.62 ($CHCl_3$/MeOH, 10:1); ^{1}H NMR (DMSO-d_6) δ 1.17 (m, 1H, CH_2), 1.40–1.62 (m, 3H, CH_2), 2.48 (m, 2H, CH_2), 2.56 (s, 3H, 2-CH_3), 3.43 (s, 3H, NCH_3), 3.98 (s, 3H, OCH_3), 6.96 (d, J = 8.2 Hz, 1H, ArH), 7.39 (d, J = 8.0 Hz, 1H, ArH), 7.54 (m, 2H, ArH), 7.64 (dd, J = 2.6 Hz, 7.6 Hz, 1H, ArH), 8.25 (dd, J = 6.2 Hz, 2.0 Hz, 1H, ArH); Anal. calcd. for ($C_{20}H_{21}N_3O$) C, H, N.

N-(5'-methoxynaphthyl-1')-N,2-dimethyl-cyclopenta[d]pyrimidin-4-amine hydrochloric acid salt (7·HCl).: 89% yield, off-white solid. mp 178.3–179.9 °C; TLC *Rf* 0.55 ($CHCl_3$/MeOH, 10:1); ^{1}H NMR (DMSO-d_6) δ 1.07 (m, 1H, CH_2), 1.52–1.66 (m, 3H, CH_2), 2.68 (s, 3H, 2-CH_3), 2.80 (m, 2H, CH_2), 3.66 (s, 3H, NCH_3), 4.02 (s, 3H, OCH_3), 7.01 (d, J = 8.0 Hz, 1H, ArH), 7.27 (d, J = 8.2 Hz, 1H, ArH), 7.55–7.60 (m, 2H, ArH), 7.67 (dd, J = 3.6 Hz, 6.2 Hz, 1H, ArH), 8.32 (d, J = 7.6 Hz, 1H, ArH); Anal. calcd. for ($C_{20}H_{22}ClN_3O\cdot 0.5EtOAc\cdot 0.45HCl$) C, H, N, Cl.

N-(6'-methoxynaphthyl-1')-N-methyl-cyclopenta[d]pyrimidin-4-amine (8).: 75% yield, off-white solid. mp 114.1–114.9 °C; TLC *Rf* 0.58 ($CHCl_3$/MeOH, 10:1); ^{1}H NMR (DMSO-d_6) δ 1.48–1.55 (m, 3H, CH_2), 2.01 (m, 1H, CH_2), 2.56 (m, 2H, CH_2), 3.47 (s, 3H, NCH_3), 3.89 (s, 3H, OCH_3), 7.19 (dd, J = 2.4 Hz, 9.0 Hz, 1H, ArH), 7.29 (d, J = 7.2 Hz, 1H, ArH), 7.45 (d, J = 2.4 Hz, 1H, ArH), 7.50 (t, J = 8.0 Hz, 1H, ArH), 7.63 (d, J = 9.5 Hz, 1H, ArH), 7.89 (d, J = 8.2 Hz, 1H, ArH), 8.50 (s, 1H, ArH); Anal. calcd. for ($C_{19}H_{19}N_3O\cdot$ 0.15EtOAc) C, H, N.

N-(5'-methoxynaphthyl-2')-N-methyl-cyclopenta[d]pyrimidin-4-amine hydrochloric salt (9·HCl).: 76% yield, off-white solid. mp 215.7–216.5 °C; TLC *Rf* 0.53 ($CHCl_3$/MeOH/TEA, 10:1:0.1); ^{1}H NMR (DMSO-d_6) δ 0.90 (m, 1H, CH_2), 1.73 (m, 3H, CH_2), 2.66 (m, 2H, CH_2), 3.66 (s, 3H, NCH_3), 4.00 (s, 3H, OCH_3), 7.07 (d, J = 7.2 Hz, 1H, ArH), 7.51–7.67 (m, 3H, ArH), 7.92 (d, J = 2.2 Hz, 1H, ArH), 8.26 (d, J = 8.2 Hz, 1H, ArH), 8.91 (s, 1H, 2-H); Anal. calcd. for ($C_{19}H_{20}ClN_3O\cdot$ 0.45H_2O) C, H, N, Cl.

N-(5'-methoxynaphthyl-2')-N-methyl-2-amino-cyclopenta[d]pyrimidin-4-amine (10).: 82% yield, off-white solid. mp 203.7–204.5 °C; TLC *Rf* 0.56 ($CHCl_3$/MeOH, 10:1); ^{1}H NMR (DMSO-d_6) δ 1.55 (m, 2H, CH_2), 1.66 (m, 2H, CH_2), 2.43 (m, 2H, CH_2), 3.44 (s, 3H, NCH_3), 3.97 (s, 3H, OCH_3), 6.07 (bs, 2H, 2-NH_2), 6.93 (dd, J = 5.0 Hz, 3.6 Hz, 1H, ArH), 7.33 (dd, J = 2.0 Hz, 9.0 Hz, 1H, ArH), 7.43 (m, 2H, ArH), 7.58 (d, J = 2.0 Hz, 1H, ArH), 8.14 (d, J = 9.2 Hz, 1H, ArH); Anal. calcd. for ($C_{19}H_{20}N_4O\cdot$ 0.25EtOAc) C, H, N.

Molecular Modeling.—Docking of compounds **4**–**10** was carried out in the published X-ray crystal structure of colchicine in tubulin (PDB: 4O2B, 2.3 Å)[22] using Schrödinger.[23] The ligands were sketched, minimized in energy and prepared using the LigPrep module of Maestro, using the default parameters. The crystal structure of tubulin was obtained from the protein database and prepared using the default parameters of Maestro and the protein preparation wizard. The receptor grid was generated using colchicine as the reference ligand. The docking was carried out with the GLIDE module with SP, flexible ligand sampling and with an output maximum of 5 poses per ligand. The docking method was validated by performing re-docking of the native ligand colchicine into the crystal structures with a RMSD of 1.04 Å. The centroid around the ligands was defined as the ligand binding site. Using prepared ligands from the Ligprep files, a conformational search was carried out to determine the number of low energy conformations within 5 kcal/mol from the minimum energy conformation. The conformational Search panel from MacroModel was used, and the settings were as follows: Force Field: OPLS3e, Solvent: water, Conformation search method: Mixed Torsional/Low-Mode sampling, and the rest of the settings were kept at default. The rotational energy barrier was calculated using the Coordinate Scan panel of Maestro. The Plot of Two-Coordinate Scan panel was used to plot the rotational energy barrier for compounds **4** and **5**. The settings were as follows: Force Field: OPLS3e, Solvent: water, Coordinate to Scan: dihedral angles around the cyclopenta[*d*]pyrimidine scaffold and the naphthyl ring (C4-N4 bond and N4-C1′ bond). The rest of the settings were kept at default.

Cell Culture.—Details about the culture of cells used in these evaluations have been described previously. [32] U251 human glioblastoma cells (PMID: 3564901) were grown in Dulbecco's modification of minimal essential media containing 10% cosmic calf serum at 37 °C with 5% CO_2 in a water jacketed incubator.

Microtubule Depolymerizing Effects.—The ability of the compounds to initiate changes in cellular microtubules was evaluated in A-10 cells because these cells arrest in interphase without the confounding effects of significant mitotic accumulation that occurs in cancer cells. Cells were treated with the compounds for 18 h and then microtubules visualized using indirect immunofluorescence. EC_{50} values were calculated as previously described[33] and represent a minimum of three independent experiments.

SRB Assay.—The SRB assay[34] was used to evaluate the antiproliferative and cytotoxic activities of the compounds in MDA-MB-435 melanoma cells as previously described.[30] The IC_{50} values represent an average of at least three independent experiments, each conducted in triplicate, plus or minus the standard deviation.

Quantitative Tubulin Studies.—Purified bovine brain tubulin was used in these studies to determine IC_{50} values for tubulin polymerization and compound inhibition of colchicine binding. The techniques used in both assays have previously been described in detail.[35] In brief, in the polymerization assay, 10 μM (1.0 mg/mL) tubulin was preincubated for 15 min at 30 °C with varying compound concentrations in 0.8 M monosodium glutamate, taken from a 2.0 M stock solution adjusted to pH 6.6 with HCl. Reaction mixtures also contained 4% (v/v) DMSO (compound solvent). Following the preincubation, reaction mixtures were placed on ice, and 10 μL of 10 mM GTP (0.4 mM final concentration) was added to each mixture. Reaction volume was 0.24 mL prior to GTP addition, and all concentrations are in terms of the final reaction volume of 0.25 mL. Reaction mixtures were transferred to 0 °C cuvettes in Beckman DU7400/7500 recording spectrophotometers equipped with electronic temperature controllers. Polymer formation was measured turbidimetrically at 350 nm. After baselines were established at 0 °C, temperature was rapidly jumped to 30 °C (less than 1 min), and the IC_{50} was defined as the compound concentration inhibiting the extent of assembly by 50% after 20 min at 30 °C. In the colchicine binding assay,[36] 0.1 mL reaction volumes contained 1.0 μM tubulin, 5.0 μM [^{3}H]colchicine (from Perkin-Elmer), and potential inhibitors at 1.0 or 5.0 μM, together with reaction components that strongly stabilize the colchicine binding activity of tubulin. Reaction mixtures also contained 5% DMSO (compound solvent). Tubulin was the last component added to the reaction mixtures, which were prepared on ice. Binding of colchicine was initiated by transferring the reaction mixtures to a 37 °C water bath, and the mixtures were incubated for 10 min (a time when the reaction without inhibitor is 40–60% complete). Reactions were stopped with ice water, and the diluted reaction mixtures were each filtered through a stack of two Whatman DEAE-cellulose filters obtained from GE Healthcare Life Sciences. Radiolabel bound to the filters was quantitated by scintillation counting.

Xenograft Study.—500,000 U251 human glioma cells were implanted into the lateral flank of NCr athymic *nu/nu* nude mice (equal numbers male/female; 8 wk age from NCI

Frederick-Charles River APA breeding stock). Maximal tolerated doses (MTDs) of compounds were determined using a 4+4 (2 male, 2 female) crossover dose escalation study starting at 5 and 10 mg/kg and escalating bi-weekly until >5% weight loss was observed. Once tumors were visible, mice were treated with the carrier (5% DMSO, 5% Kolliphor-15, 90% normal saline), MTD of temozolomide (50 mg/kg/wk) or MTD of compound **5** (17.5 mg/kg/2x wk) until the end of the experiment. Data were obtained from 6–8 animals. Tumor size was assessed by measuring tumor length, width, and depth twice weekly using Vernier calipers. Tumor volume was calculated with the ellipsoid formula: volume = 0.52 (length × width × depth). Animal weights were assessed twice weekly in all treatment groups until the end of the study.

Supplementary Material

Refer to Web version on PubMed Central for supplementary material.

ACKNOWLEDGEMENTS

The work was supported, in part, by a grant from the National Institutes of Health, National Cancer Institute, R01 CA142868 (AG and SLM), the Duquesne University Adrian Van Kaam Chair in Scholarly Excellence (A.G.) and the Greehey Chair (SLM). This research was supported in part by the Developmental Therapeutics Program in the Division of Cancer Treatment and Diagnosis of the National Cancer Institute, which includes federal funds under Contract No. HHSN261200800001E. The content of this publication does not necessarily reflect the views or policies of the Department of Health and Human Services, nor does mention of trade names, commercial products, or organizations imply endorsement by the U.S. Government.

ABBREVIATIONS

CA-4	Combretastatin A-4
Pgp	P-glycoprotein
SRB	sulforhodamine
B MTA	Microtubule Targeting Agent
DMSO	dimethyl sulfoxide

REFERENCES

1. Jordan MA; Wilson L, Microtubules as a target for anticancer drugs. Nat Rev Cancer 2004, 4 (4), 253–65. [PubMed: 15057285]
2. Borisy G; Heald R; Howard J; Janke C; Musacchio A; Nogales E, Microtubules: 50 years on from the discovery of tubulin. Nat Rev Mol Cell Biol 2016, 17 (5), 322–8. [PubMed: 27103327]
3. Dumontet C; Jordan MA, Microtubule-binding agents: a dynamic field of cancer therapeutics. Nat Rev Drug Discov 2010, 9 (10), 790–803. [PubMed: 20885410]
4. Bates D; Eastman A, Microtubule destabilising agents: far more than just antimitotic anticancer drugs. Br J Clin Pharmacol 2017, 83 (2), 255–268. [PubMed: 27620987]
5. Kaul R; Risinger AL; Mooberry SL, Microtubule-targeting drugs: more than antimitotics. J Nat Prod 2019, 82 (3), 680–685. [PubMed: 30835122]
6. Steinmetz MO; Prota AE, Microtubule-targeting agents: strategies to hijack the cytoskeleton. Trends Cell Biol 2018, 28 (10), 776–792. [PubMed: 29871823]

7. Prota AE; Bargsten K; Northcote PT; Marsh M; Altmann KH; Miller JH; Diaz JF; Steinmetz MO, Structural basis of microtubule stabilization by laulimalide and peloruside A. Angew Chem Int Ed Engl 2014, 53 (6), 1621–5. [PubMed: 24470331]
8. Meyer CJ; Krauth M; Wick MJ; Shay JW; Gellert G; De Brabander JK; Northcote PT; Miller JH, Peloruside A inhibits growth of human lung and breast tumor xenografts in an athymic nu/nu mouse model. Mol Cancer Ther 2015, 14 (8), 1816–23. [PubMed: 26056149]
9. Sievers EL; Senter PD, Antibody-drug conjugates in cancer therapy. Annu Rev Med 2013, 64, 15–29. [PubMed: 23043493]
10. Lu Y; Chen J; Xiao M; Li W; Miller DD, An overview of tubulin inhibitors that interact with the colchicine binding site. Pharm Res 2012, 29 (11), 2943–2971. [PubMed: 22814904]
11. Xia LY; Zhang YL; Yang R; Wang ZC; Lu YD; Wang BZ; Zhu HL, Tubulin inhibitors binding to colchicine-site: a review from 2015 to 2019. Curr Med Chem 2019.
12. Prota AE; Bargsten K; Diaz JF; Marsh M; Cuevas C; Liniger M; Neuhaus C; Andreu JM; Altmann KH; Steinmetz MO, A new tubulin-binding site and pharmacophore for microtubule-destabilizing anticancer drugs. Proc Natl Acad Sci U S A 2014, 111 (38), 13817–21. [PubMed: 25114240]
13. Kavallaris M, Microtubules and resistance to tubulin-binding agents. Nat Rev Cancer 2010, 10 (3), 194–204. [PubMed: 20147901]
14. Parker AL; Teo WS; McCarroll JA; Kavallaris M, An Emerging role for tubulin isotypes in modulating cancer biology and chemotherapy resistance. Int J Mol Sci 2017, 18 (7).
15. Prassanawar SS; Panda D, Tubulin heterogeneity regulates functions and dynamics of microtubules and plays a role in the development of drug resistance in cancer. Biochem J 2019, 476 (9), 1359–1376. [PubMed: 31085712]
16. Stengel C; Newman SP; Leese MP; Potter BVL; Reed MJ; Purohit A, Class III beta-tubulin expression and in vitro resistance to microtubule targeting agents. Br J Cancer 2010, 102 (2), 316–324. [PubMed: 20029418]
17. Wu X; Wang Q; Li W, Recent advances in heterocyclic tubulin inhibitors targeting the colchicine binding site. Anticancer Agents Med Chem 2016, 16 (10), 1325–1338. [PubMed: 26899186]
18. Gangjee A; Zhao Y; Lin L; Raghavan S; Roberts EG; Risinger AL; Hamel E; Mooberry SL, Synthesis and discovery of water-soluble microtubule targeting agents that bind to the colchicine site on tubulin and circumvent Pgp mediated resistance. J Med Chem 2010, 53 (22), 8116–8128. [PubMed: 20973488]
19. Xiang W; Choudhary S; Hamel E; Mooberry SL; Gangjee A, Structure based drug design and in vitro metabolism study: Discovery of N-(4-methylthiophenyl)-N,2-dimethyl-cyclopenta[d]pyrimidine as a potent microtubule targeting agent. Bioorg Med Chem 2018, 26 (9), 2437–2451. [PubMed: 29655610]
20. Gangjee A; Zhao Y; Raghavan S; Rohena CC; Mooberry SL; Hamel E, Structure-activity relationship and in vitro and in vivo evaluation of the potent cytotoxic anti-microtubule agent N-(4-Methoxyphenyl)-N,2,6-trimethyl-6,7-dihydro-5H-cyclopenta[d]pyrimidin-4-aminium chloride and its analogues as antitumor agents. J Med Chem 2013, 56 (17), 6829–6844. [PubMed: 23895532]
21. Gangjee A; Zhao Y; Hamel E; Westbrook C; Mooberry SL, Synthesis and biological activities of (R)- and (S)-N-(4-Methoxyphenyl)-N,2,6-trimethyl-6,7-dihydro-5H-cyclopenta[d]pyrimidin-4-aminium chloride as potent cytotoxic antitubulin agents. J Med Chem 2011, 54 (17), 6151–6155. [PubMed: 21786793]
22. Prota AE; Danel F; Bachmann F; Bargsten K; Buey RM; Pohlmann J; Reinelt S; Lane H; Steinmetz MO, The novel microtubule-destabilizing drug BAL27862 binds to the colchicine site of tubulin with distinct effects on microtubule organization. J Mol Biol 2014, 426 (8), 1848–60. [PubMed: 24530796]
23. Small-Molecule Drug Discovery Suite 2020–1, S, LLC, New York, NY, 2020
24. Lee L; Robb LM; Lee M; Davis R; Mackay H; Chavda S; Babu B; O'Brien EL; Risinger AL; Mooberry SL; Lee M, Design, synthesis, and biological evaluations of 2,5-diaryl-2,3-dihydro-1,3,4-oxadiazoline analogs of combretastatin-A4. J Med Chem 2010, 53 (1), 325–334. [PubMed: 19894742]

25. Cognet JAH; Boulard Y; Fazakerley GV, Helical parameters, fluctuations, alternative hydrogen bonding, and bending in oligonucleotides containing a mistmatched base-pair by NOESY distance restrained and distance free molecular dynamics. J Mol Biol 1995, 246 (1), 209–226. [PubMed: 7853398]
26. Kaluarachchi K; Meadows RP; Gorenstein DG, How accurately can oligonucleotide structures be determined from the hybrid relaxation rate matrix/NOESY distance restrained molecular dynamics approach? Biochemistry 1991, 30 (36), 8785–8797. [PubMed: 1888738]
27. Mishra SH; Harden BJ; Frueh DP, A 3D time-shared NOESY experiment designed to provide optimal resolution for accurate assignment of NMR distance restraints in large proteins. J Biomol NMR 2014, 60 (4), 265–274. [PubMed: 25381567]
28. Mumenthaler C; Braun W, Automated assignment of simulated and experimental NOESY spectra of proteins by feedback filtering and self-correcting distance geometry. J Mol Biol 1995, 254 (3), 465–480. [PubMed: 7490763]
29. Butts CP; Jones CR; Towers EC; Flynn JL; Appleby L; Barron NJ, Interproton distance determinations by NOE – surprising accuracy and precision in a rigid organic molecule. Org Biomol Chem 2011, 9 (1), 177–184. [PubMed: 21042643]
30. Risinger AL; Jackson EM; Polin LA; Helms GL; LeBoeuf DA; Joe PA; HopperBorge E; Luduena RF; Kruh GD; Mooberry SL, The taccalonolides: microtubule stabilizers that circumvent clinically relevant taxane resistance mechanisms. Cancer Res 2008, 68 (21), 8881–8888. [PubMed: 18974132]
31. Golani LK; Islam F; O'Connor C; Dekhne AS; Hou Z; Matherly LH; Gangjee A, Design, synthesis and biological evaluation of novel pyrrolo[2,3-d]pyrimidine as tumor-targeting agents with selectivity for tumor uptake by high affinity folate receptors over the reduced folate carrier. Bioorg Med Chem 2020, 28 (12), 115544.
32. Rohena CC; Telang NS; Da C; Risinger AL; Sikorski JA; Kellogg GE; Gupton JT; Mooberry SL, Biological characterization of an improved pyrrole-based colchicine site agent identified through structure-based design. Mol Pharmacol 2016, 89 (2), 287–96. [PubMed: 26655304]
33. Lee L; Robb LM; Lee M; Davis R; Mackay H; Chavda S; Babu B; O'Brien EL; Risinger AL; Mooberry SL; Lee M, Design, synthesis, and biological evaluations of 2,5-diaryl-2,3-dihydro-1,3,4-oxadiazoline analogs of combretastatin-A4. J Med Chem 2010, 53 (1), 325–334. [PubMed: 19894742]
34. Skehan P; Storeng R; Scudiero D; Monks A; McMahon J; Vistica D; Warren JT; Bokesch H; Kenney S; Boyd MR, New colorimetric cytotoxicity assay for anticancer-drug screening. J Natl Cancer Inst 1990, 82 (13), 1107–12. [PubMed: 2359136]
35. Hamel E, Evaluation of antimitotic agents by quantitative comparisons of their effects on the polymerization of purified tubulin. Cell Biochem Biophys 2003, 38 (1), 1–21. [PubMed: 12663938]
36. Verdier-Pinard P; Lai JY; Yoo HD; Yu J; Marquez B; Nagle DG; Nambu M; White JD; Falck JR; Gerwick WH; Day BW; Hamel E, Structure-activity analysis of the interaction of curacin A, the potent colchicine site antimitotic agent, with tubulin and effects of analogs on the growth of MCF-7 breast cancer cells. Mol Pharmacol 1998, 53 (1), 62–76. [PubMed: 9443933]

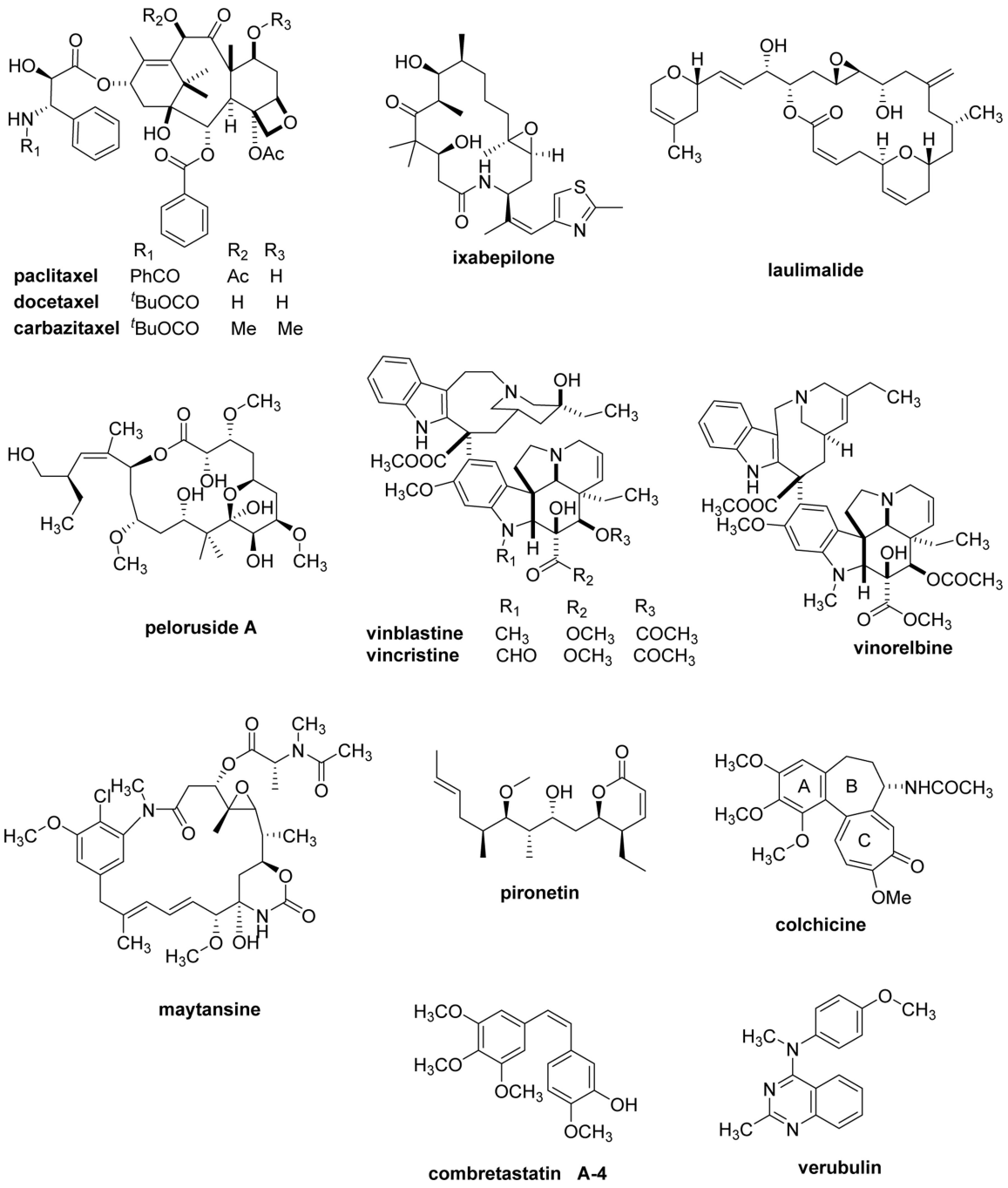

Figure 1.
Structures of microtubule targeting agents.

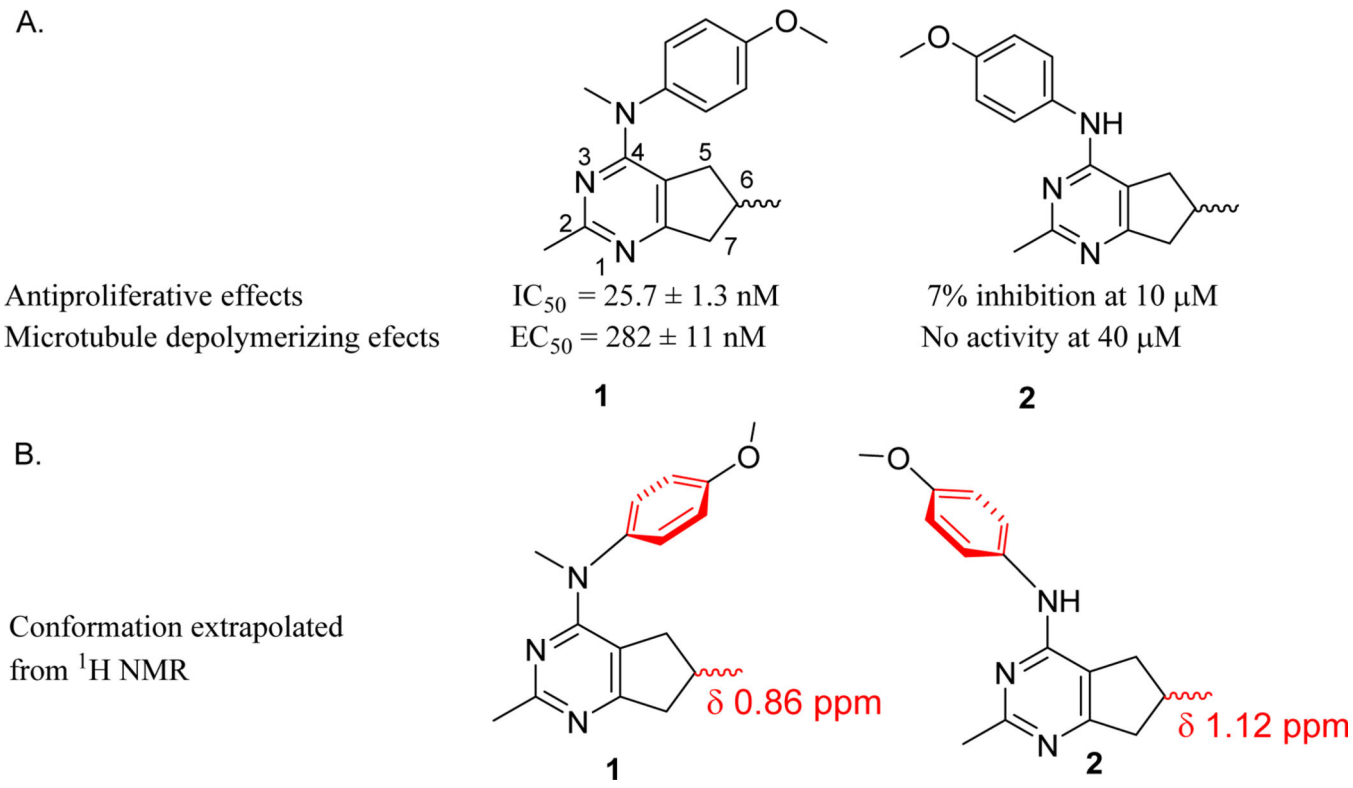

Figure 2.

A. Compounds **1** and **2** and their antiproliferative activities and disassembly effects on microtubules. B. The general conformation of the aniline ring towards (**1**) and away (**2**) from the cyclopenta[*d*]pyrimidine ring from ^{1}H NMR.

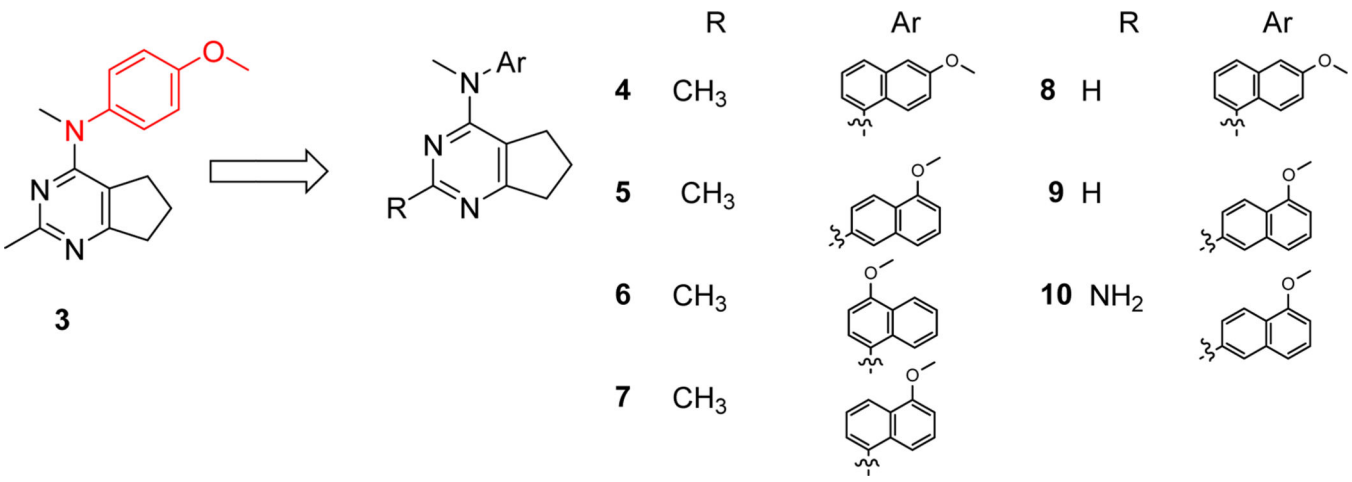

Figure 3.
Compound **3** and the designed analogs **4–10**.

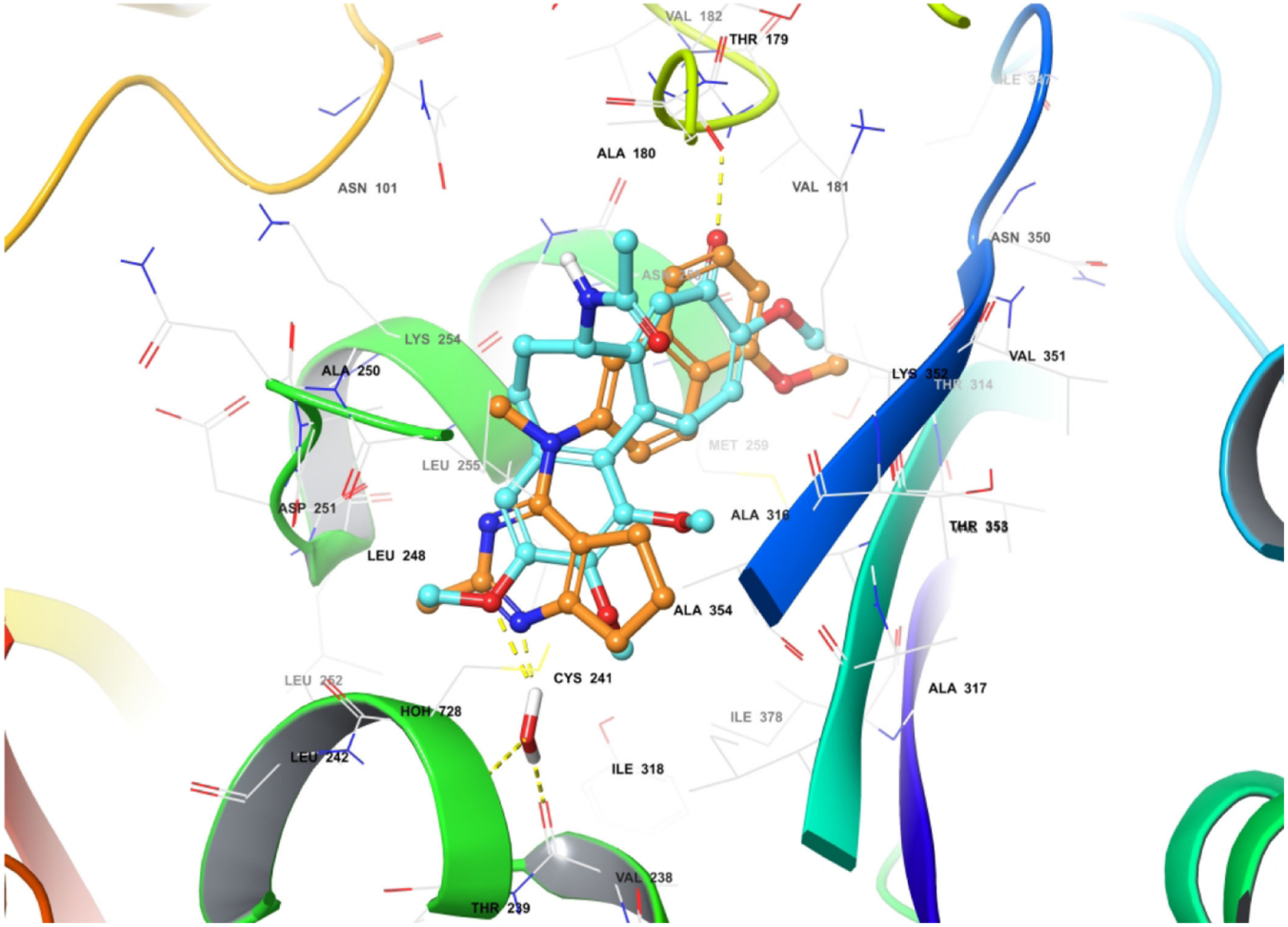

Figure 4.

Superimposition of the docked pose of **5** (tan) in the colchicine site (colchicine in cyan) of tubulin (PDB: 4O2B[22]).

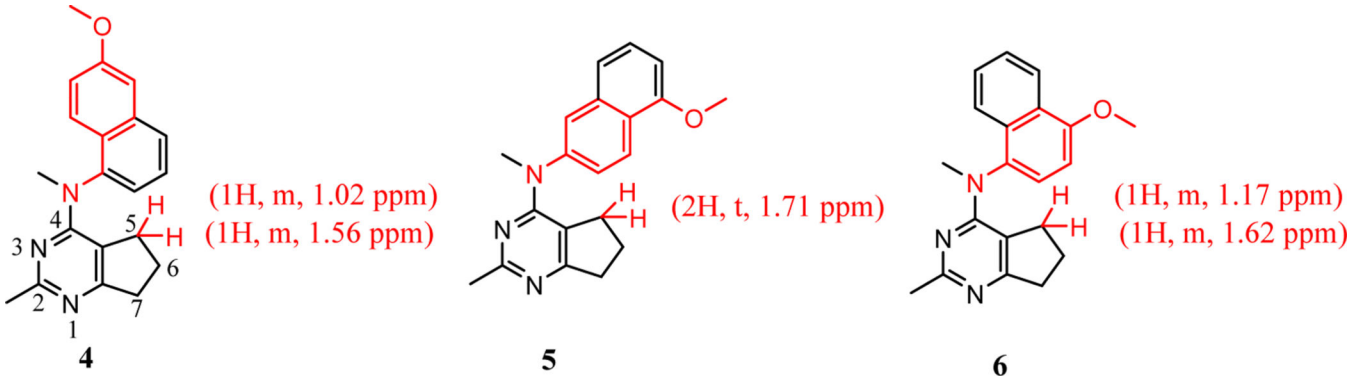

4 **5** **6**

Figure 5.

Chemical shift and coupling pattern (^{1}H NMR, DMSO-d6 and D_2O (1:1)) of the 5-C**H**$_2$ in compounds **4**–**6**.

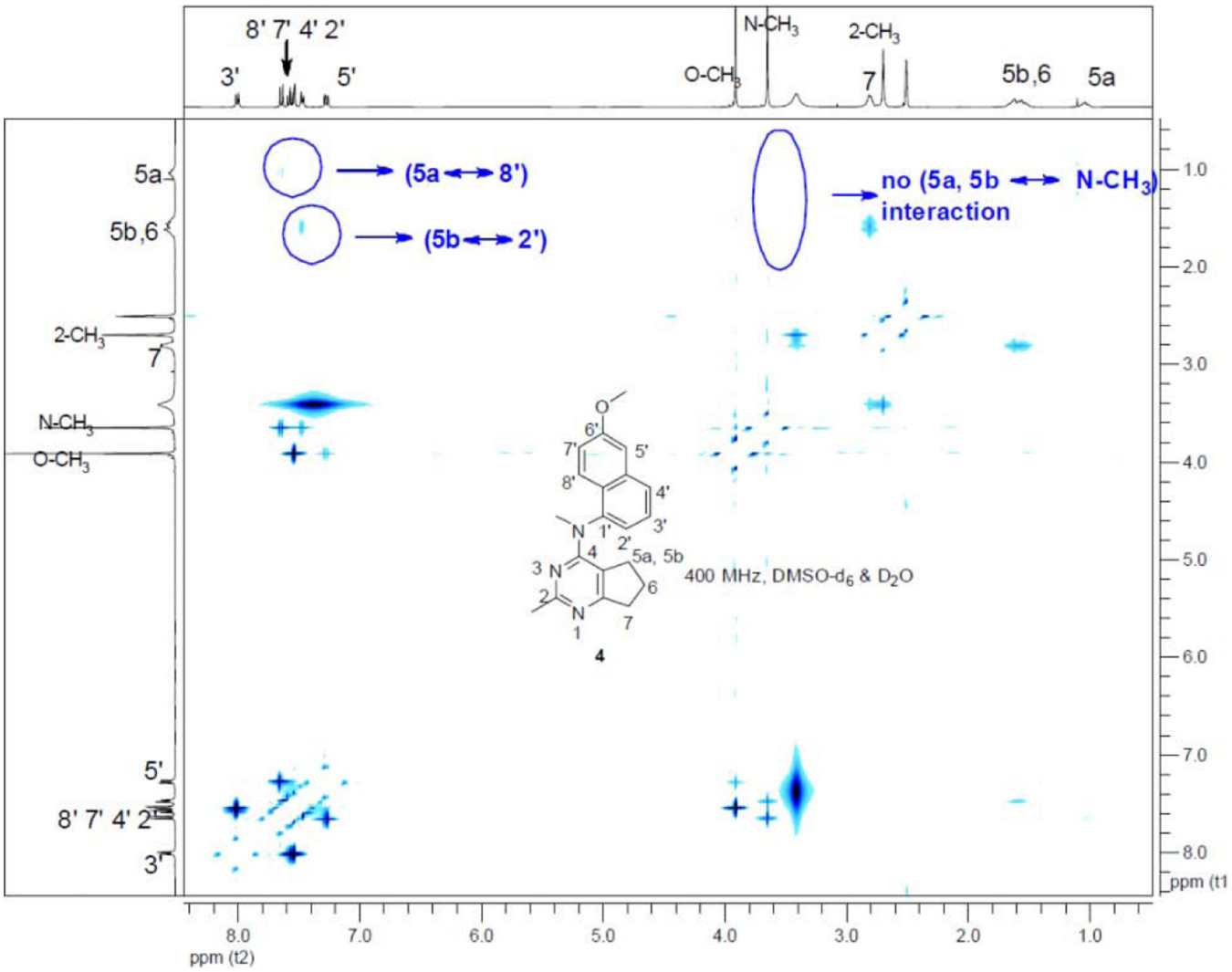

Figure 6A.
NOESY study of **4** and spectrum interpretation.

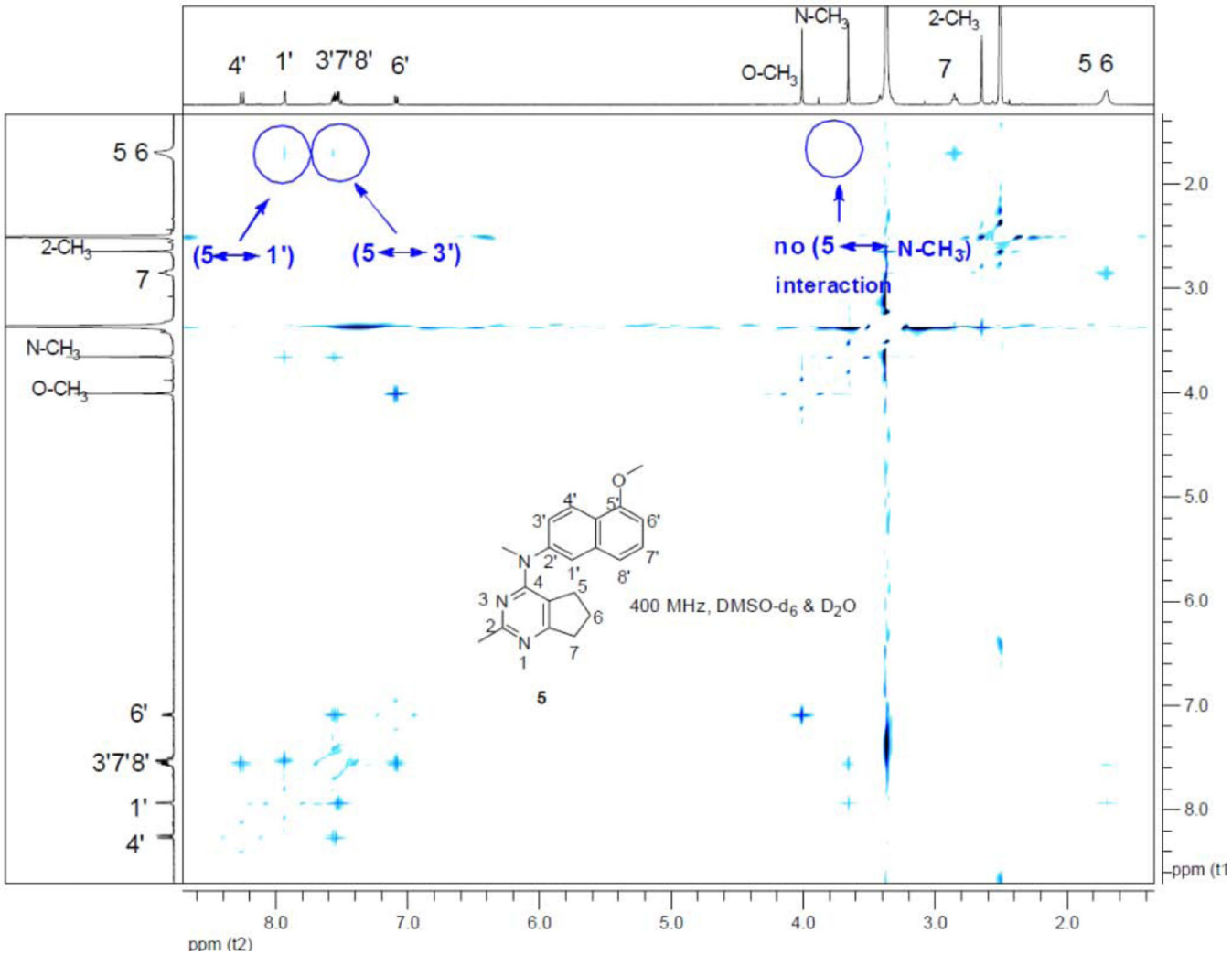

Figure 6B.
NOESY study of **5** and spectrum interpretation.

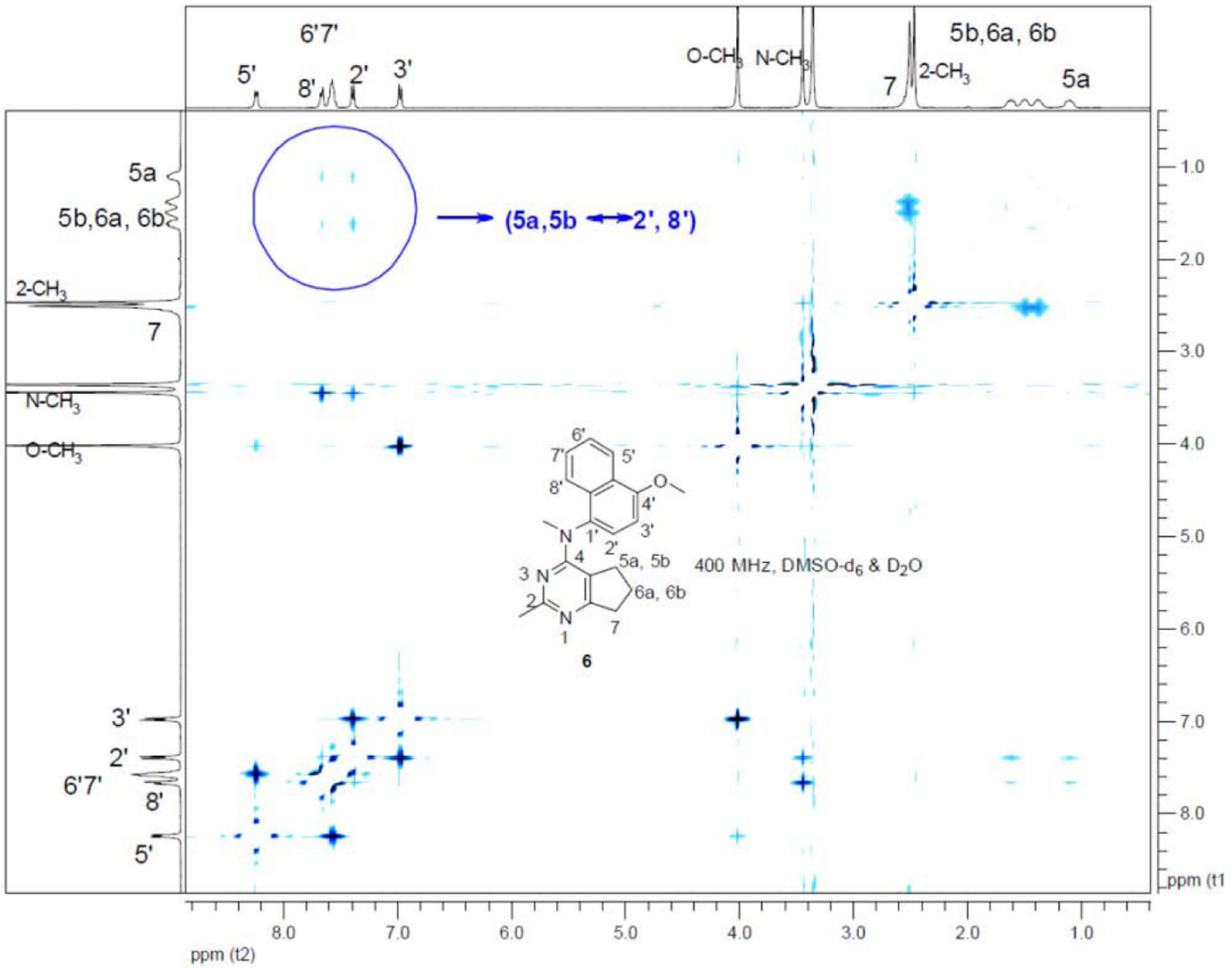

Figure 6C.
NOESY study of **6** and spectrum interpretation.

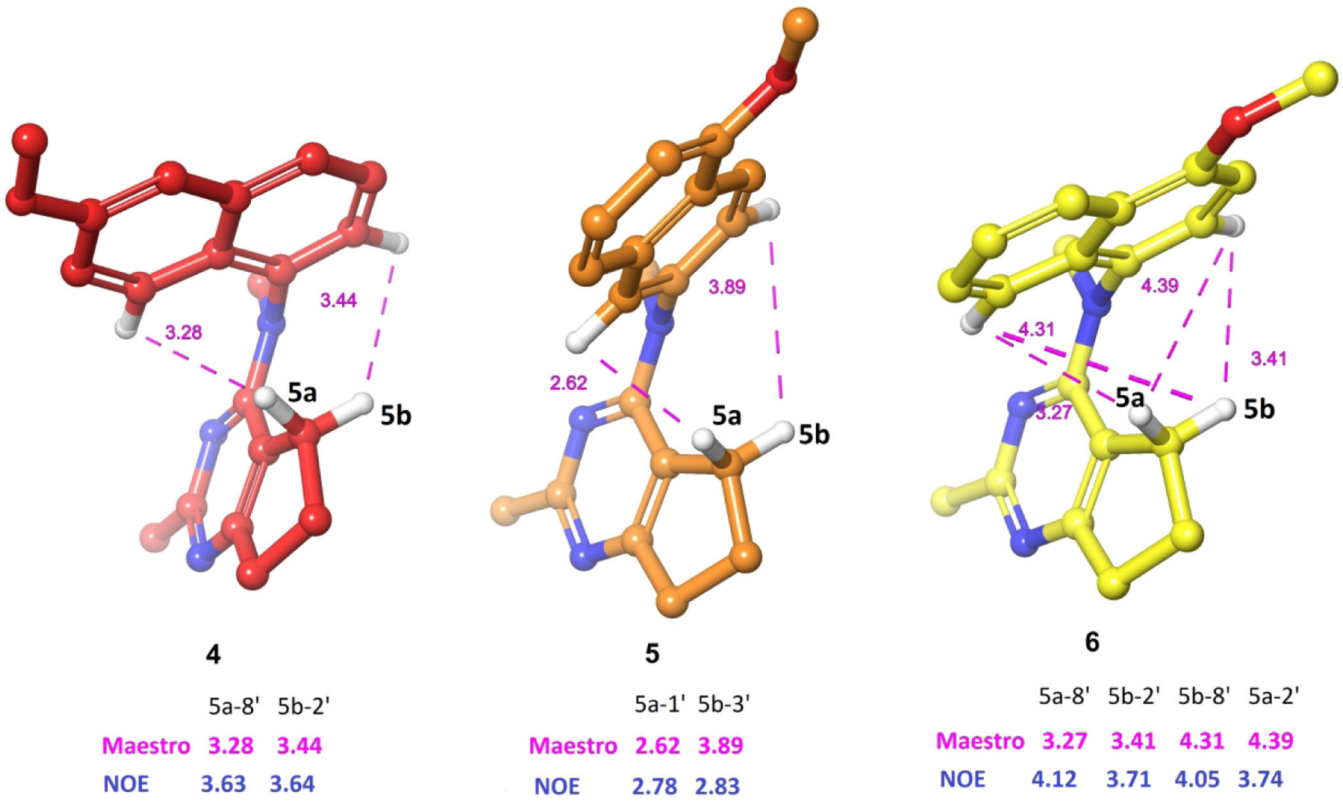

Figure 7.

Lowest energy conformations of **4**–**6** simulated by Maestro 2020–1. The distance measured by Maestro in Å is in magenta. The distance in blue is the NOE calculated distance.

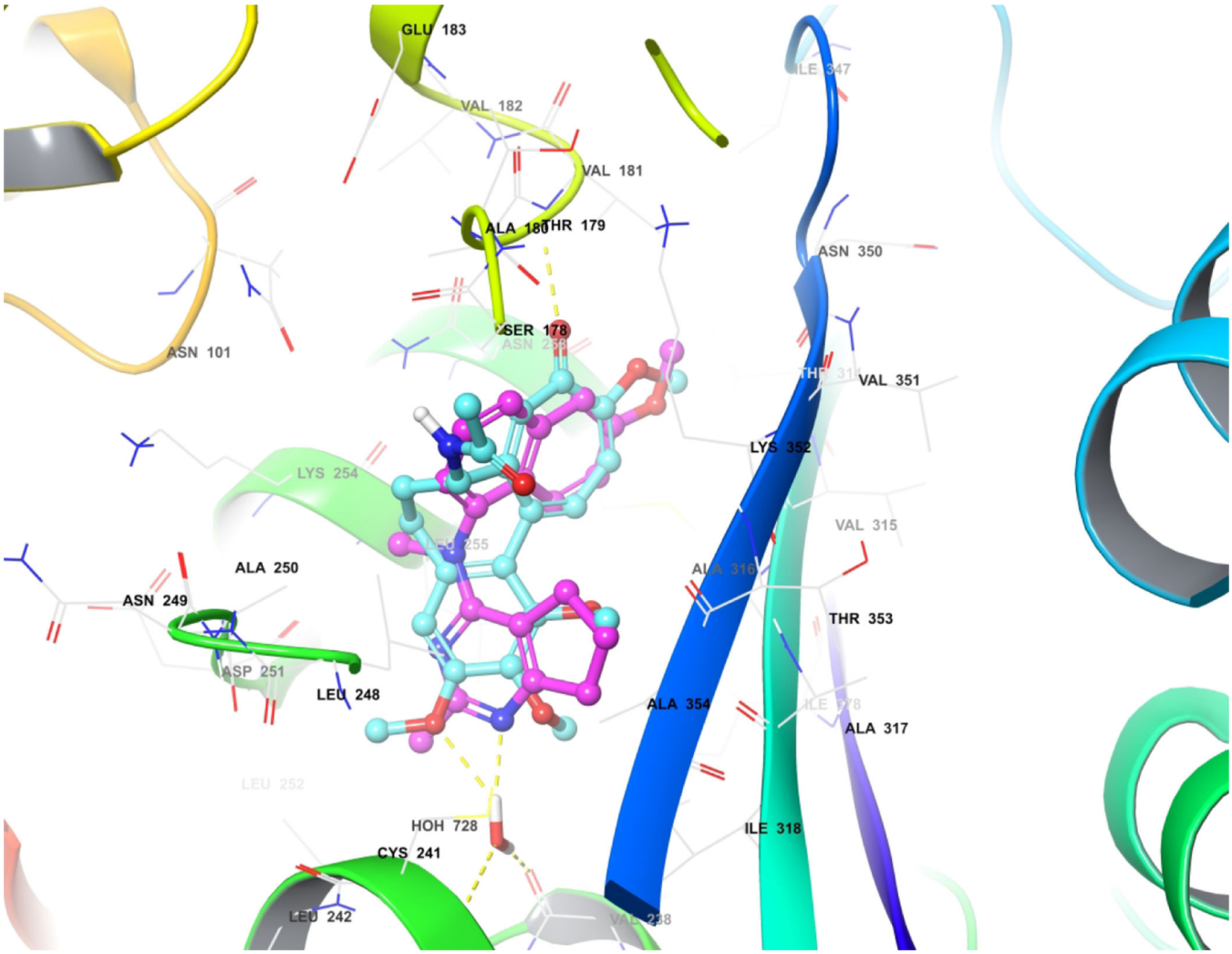

Figure 8.

Superimposition of the docked pose of **4** (magenta) in the colchicine site (colchicine in cyan) of tubulin (PDB: 4O2B[22]).

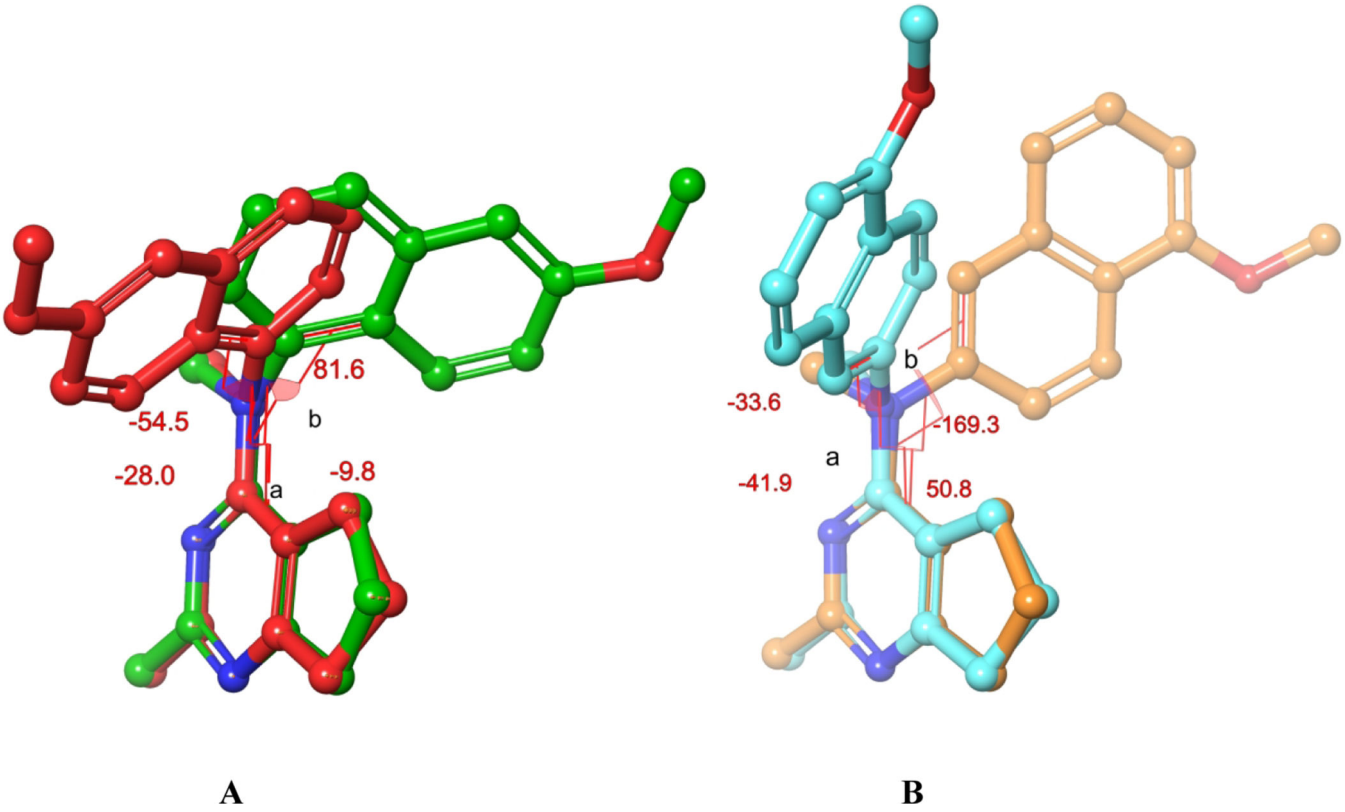

Figure 9.

A. Superimposition of the energy minimized conformation (red) of **4** and the docked conformation of **4** (green) in the colchicine site of tubulin (PDB: 4O2B[22]). B. Superimposition of the energy minimized conformation of **5** (cyan) and the docked conformation of **5** (tan) in the colchicine site of tubulin (PDB: 4O2B[22]).

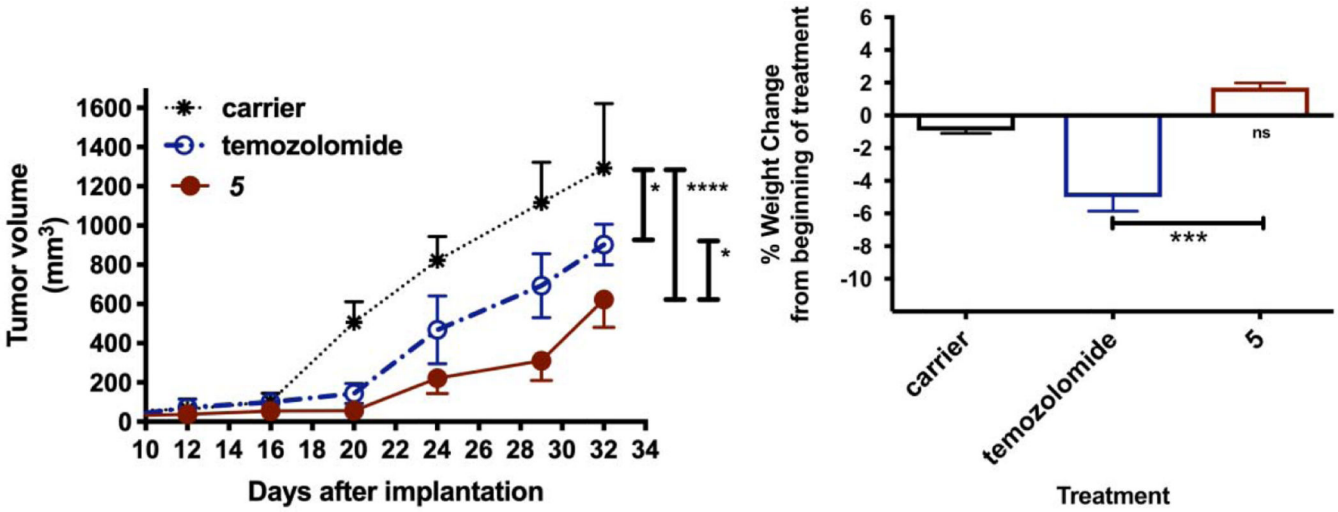

Figure 10.

Treatment with compound **5** inhibited tumor growth with little change in animal weight in a U251 flank xenograft model. *, P < 0.05; **, P < 0.01; ***, P < 0.001. U251 human glioma cells (500,000) were implanted into the lateral flank of NCr athymic nu/nu nude mice, and the mice were treated with carrier (5% DMSO, 5% Kolliphor-15, 90% normal saline), temozolomide (50 mg/kg/wk) or compound **5** (17.5 mg/kg twice week, the previously defined MTDs, until the end of the experiment. Data were obtained from 6–8 animals. (Left Panel) Tumor size was assessed by measuring tumor length, width, and depth twice weekly using Vernier calipers. Tumor volume was calculated with the ellipsoid formula: volume = 0.52 (length × width × depth) and graphically represented as days after implantation. Statistical analysis was performed using a two-way ANOVA with repeated measures post-test. (Right Panel) Graphical representation of percent change in animal weight at the beginning and end of the experiment. Statistical analysis was performed using a one-way ANOVA with a Bonferroni post-test. Drug administration was initiated 7 days after tumor implantation and continued until the end of the study.

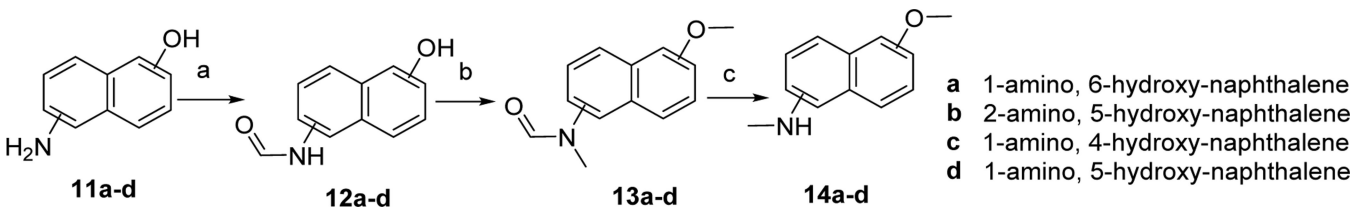

Scheme 1.

Synthesis of methoxy *N*-methyl naphthylamines **14a-d**.

Reagents and conditions: (a) HCOOH, Ac_2O, DCM, rt, 18 h; (b) NaH, MeI, DMF, 0 °C, 4 h, 71–90% (2 steps); (c) HCl (conc.), reflux, 2 h, 90 – 95%.

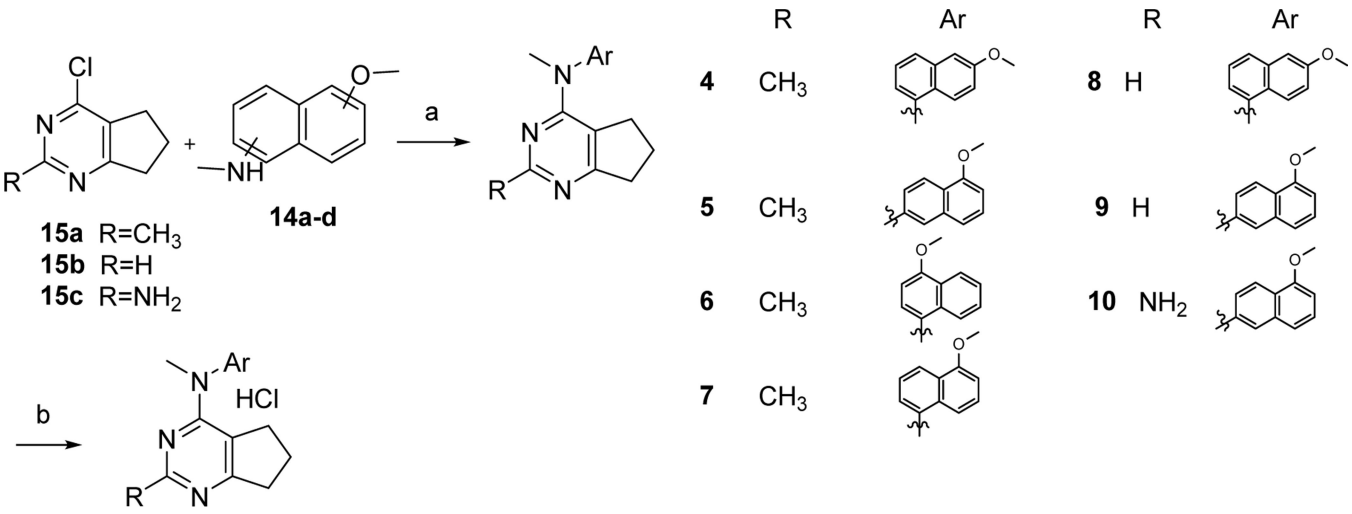

Scheme 2.

Synthesis of target compounds **4**–**10**.

Reagents and conditions: (a) Dioxane, 110 °C, 3–6 h, 71–93%; (b) MtBE, HCl (2 N in Et_2O), 90–97%.

Table 1.

EC_{50} values for the microtubule depolymerization and IC_{50} values for the inhibition of proliferation of MDA-MB-435 cancer cells.

Compound	EC_{50} (nM)	IC_{50} ± SD (nM)
3	26	7.0 ± 0.7
4	>10000	ND[a]
5	4.5	2.8 ± 0.2
6	500	230 ± 20
7	3700	820 ± 72
8	>10000	ND[a]
9	184	34.0 ± 3.4
10	26	8.7 ± 0.6
CA-4	13	3.4 ± 0.6

[a]ND: Not determined

Table 2.

Cytotoxicity of compounds **4–9** in the U251 cancer cells.

Compound	IC_{50} ± SD (nM) in U251 cells
4	88.3 ± 14.2
5	17.6 ± 2.1
6	35.1 ± 5.0
7	38.9 ± 5.9
8	132.6 ± 15.0
9	72.5 ± 8.8

Table 3.

Inhibition of tubulin assembly and colchicine binding by CA-4 and **4–10**.

Compound	Inhibition of tubulin assembly IC_{50} (μM) ± SD	Inhibition of colchicine binding % Inhibition ± SD	
		5 μM inhibitor	1 μM inhibitor
3	1.6 ± 0.1	92 ± 0.7	70 ± 2
4	> 20	ND[a]	ND[a]
5	0.98 ± 0.04	98 ± 0.3	86 ± 0.7
6	1.4 ± 0.007	72 ± 0.6	ND[a]
8	> 20	ND[a]	ND[a]
9	1.2 ± 0.04	93 ± 0.6	77 ± 1
CA-4	1.3 ± 0.1	98 ± 0.6	87 ± 0.2

[a]ND: Not determined

Table 4.

Compound **3**, **5**–**7**, and **9**–**10** circumvent βIII-Tubulin Mediated Resistance.

Compd.	IC_{50} (nM) ± SD		
	HeLa	βIII Expressing HeLa	Rr*
3	12.0 ± 1.2	9.6 ± 0.9	0.8
5	3.4 ± 0.4	2.6 ± 0.4	0.8
6	250 ± 14	180 ± 11	0.7
7	1200 ± 110	780 ± 60	0.7
9	56.4 ± 8	43 ± 2	0.8
10	12.6 ± 0.6	9.6 ± 0.6	0.8
CA-4	4.7 ± 0.2	5.7 ± 0.4	1.2
Paclitaxel	1.6 ± 0.2	7.7 ± 0.2	4.7

*Relative resistance. The Rr was calculated by dividing the IC_{50} of the βIII expressing HeLa cell line (WTβIII) by the IC_{50} of the parental HeLa cells

Table 5.

Compound **3**, **5**–**7**, and **9**–**10** circumvent Pgp Mediated Resistance.

Compd.	IC_{50} (nM) ± SD		
	SK-OV-3	SK-OV-3 MDR-1-6/6	Rr*
3	11.3 ± 0.2	16.4 ± 0.4	1.5
5	2.7 ± 0.1	5.7 ± 1.7	2.1
6	330 ± 27	400 ± 74	1.2
7	1200 ± 110	1300 ± 100	1.1
9	37 ± 7	74 ± 19	2.0
10	14.9 ± 0.6	19.6 ± 1.5	1.3
CA-4	4.5 ± 0.2	6.6 ± 1.3	1.5
Paclitaxel	3.0 ± 0.06	2600 ± 270	864

*Relative resistance. The Rr was calculated by dividing the IC_{50} of the Pgp expressing cells (SK-OV-3 MDR-1–6/6) by the IC_{50} of the parental SK-OV-3 cells